

NAT'L INST. OF STAND & TECH
A11106 053239

NIST
PUBLICATIONS

REFERENCE

NISTIR 6754

Effect of Bulk Lubricant Concentration on the Excess Surface Density During R123 Pool Boiling

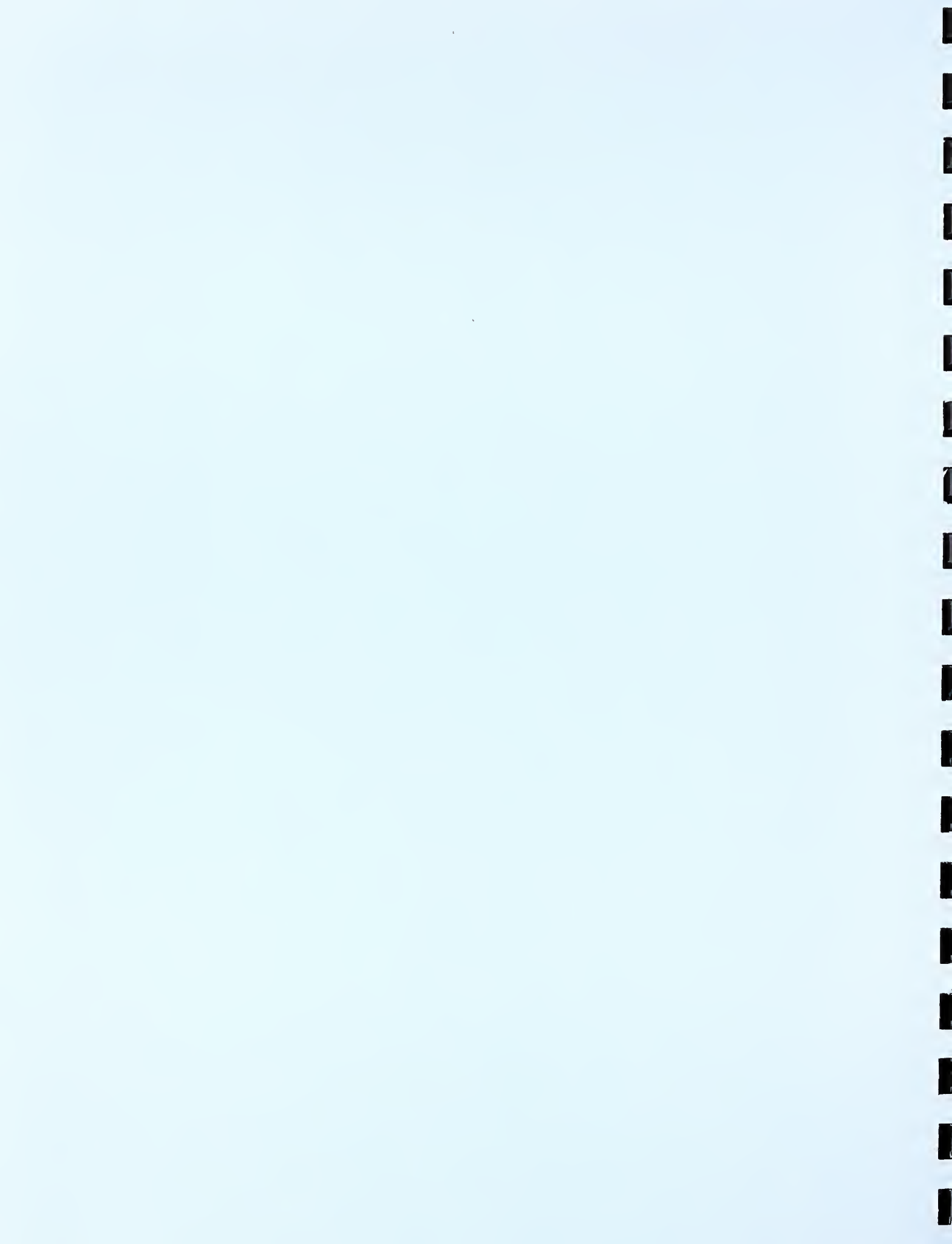
M. A. Kedzierski

U. S. DEPARTMENT OF COMMERCE
Technology Administration
National Institute of Standards
and Technology
Building and Fire Research Lab
Gaithersburg, MD 20899-8230

QC
100
.U56
No. 6754
2001



NIST
**National Institute of Standards
and Technology**
Technology Administration
U.S. Department of Commerce



Effect of Bulk Lubricant Concentration on the Excess Surface Density During R123 Pool Boiling

M. A. Kedzierski

U. S. DEPARTMENT OF COMMERCE
Technology Administration
National Institute of Standards
and Technology
Building and Fire Research Lab
Gaithersburg, MD 20899-8230

July 20, 2001



U.S. DEPARTMENT OF COMMERCE
Donald L. Evans, Secretary

NATIONAL INSTITUTE OF STANDARDS
AND TECHNOLOGY
Dr. Karen H. Brown, Acting Director

Effect of Bulk Lubricant Concentration on the Excess Surface Density During R123 Pool Boiling

M. A. Kedzierski
National Institute of Standards and Technology
Bldg. 226, Rm B114
Gaithersburg, MD 20899
Phone: (301) 975-5282
Fax: (301) 975-8973

ABSTRACT

This paper investigates the effect that bulk lubricant concentration has on the non-adiabatic lubricant excess surface density on a roughened, horizontal flat pool-boiling surface. Both pool boiling heat transfer data and lubricant excess surface density data are given for pure R123 and three different mixtures of R123 and a naphthenic mineral oil. A spectrofluorometer was used to measure the lubricant excess density that was established by the boiling of a R123/lubricant mixture on a test surface. The fluorescent technique was used to measure the effect of bulk lubricant concentration on the lubricant excess layer during refrigerant/lubricant mixture boiling. The lubricant is preferentially drawn out of the bulk refrigerant/lubricant mixture by the boiling process and accumulates on the surface in excess of the bulk concentration. The excess lubricant resides in a very thin layer on the surface and influences the boiling performance. Accordingly, the ability to measure the effect of bulk lubricant composition on the lubricant excess density and in turn the effect on the heat transfer would lead to a fundamental understanding of the mechanism by which lubricants can degrade or improve boiling performance. In support of this effort, heat transfer data are provided for pure R123 and three R123/lubricant mixtures at 277.6 K. The heat transfer data shows that the lubricant excess causes an average enhancement of the heat flux of 9 % and 5 % for the 0.5 % and 1 % lubricant mass fractions, respectively, and an average degradation of 12 % in the heat flux for the 1.8 % lubricant mass fraction mixture.

Keywords: adsorption, alternative refrigerants, boiling, enhanced heat transfer, fluorescence, non-adiabatic lubricant excess surface density, pool boiling, R123, refrigerant/lubricant mixtures, smooth surface, surfactant

1

¹ Certain trade names and company products are mentioned in the text or identified in an illustration in order to adequately specify the experimental procedure and equipment used. In no case does such an identification imply recommendation or endorsement by the National Institute of Standards and Technology, nor does it imply that the products are necessarily the best available for the purpose.

INTRODUCTION

The addition of lubricant to refrigerant can significantly alter the boiling performance due to lubricant accumulation at the heat transfer surface. Stephan (1963) was one of the first researchers to note that a lubricant-rich layer exists near the tube wall. The excess concentration (excess surface density) arises from the low vapor pressure of the lubricant relative to the refrigerant. The lubricant can be locally drawn out of solution as a consequence of refrigerant evaporation at the heat transfer surface. The refrigerant/lubricant liquid mixture travels to the heated wall, and the refrigerant preferentially evaporates from the surface leaving behind a liquid phase enriched in lubricant. A balance between deposition and removal of the lubricant establishes the thickness of the excess lubricant at the surface. It is hypothesized that the lubricant excess layer controls the bubble size, the site density and, in turn, the magnitude of the heat transfer.

Kedzierski (2001) developed a fluorescence measurement technique to verify the existence of the lubricant excess layer during pool boiling. A spectrofluorometer was specially adapted for use with a bifurcated optical bundle so that fluorescence measurements could be made perpendicular to the heat transfer surface. The study suggested that the excess layer was pure lubricant with a thickness ranging from 0.04 mm to 0.06 mm depending on the heat flux. The study examined only one refrigerant/lubricant mixture.

The present study uses the measurement technique to extend the database to three R123/York-C™ mixtures with different mass compositions: 99.5/0.5, 99/1, and 98.2/1.8. In the present study, pure R123 and R123/lubricant mixtures were tested in an effort to investigate influence of bulk lubricant concentration on the lubricant excess surface density. A naphthenic mineral oil (York-C™) was chosen for its somewhat favorable fluorescence characteristics and to demonstrate the use of the new measurement technique with a commercial lubricant.

APPARATUS

Figure 1 shows a schematic of the apparatus that was used to measure the pool boiling data of this study. More specifically, the apparatus was used to measure the liquid saturation temperature (T_s), the average pool-boiling heat flux (q''), the wall temperature (T_w) of the test surface, and the fluorescence intensity from the boiling surface (F). The three principal components of the apparatus were test chamber, condenser, and purger. The internal dimensions of the test chamber were 25.4 mm × 257 mm × 1.54 m. The test chamber was charged with approximately 7 kg of R123 from the purger, giving a liquid height of approximately 80 mm above the test surface. As shown in Fig. 1, the test section was visible through two opposing, flat 150 mm × 200 mm quartz windows. The bottom of the test surface was heated with high velocity (2.5 m/s) water flow. The vapor produced by liquid boiling on the test surface was condensed by the brine-cooled, shell-and-tube condenser and returned as liquid to the pool by gravity.

Figure 2 shows a view of the spectrofluorometer that was used to make the fluorescence measurements and the test chamber with the fluorescence probe perpendicular to the heat

transfer surface. Figure 3 shows a simplified schematic of the right angle spectrofluorometer consisting of a xenon light source, an excitation and an emission monochromator, and an emission photomultiplier tube (detector). The light source was focused into the excitation monochromator by a collimating lens. The monochromator was set to emit light at a wavelength of 380 nm. Because the intensity of the xenon lamp varies with wavelength, a corrected excitation module was used to compensate for the variation. The light from the excitation monochromator passed through a 2.5 nm slit before it entered the sample chamber. All of the slit widths were 2.5 nm to limit the bandwidth of the wavelength. The spectrofluorometer was designed to accept 45 mm × 10 mm × 10 mm fluorescent samples or cuvettes filled with fluorescent material. A special adapter with lenses and mirrors, which replaced the cuvette holder, was fabricated to allow the optical bundles to communicate with the standard sample chamber of the spectrofluorometer. The adapter was configured to direct excitation to the test surface and the emission light from the test surface to the detector. A glass filter was placed before the emission monochromator to keep light with wavelengths less than 420 nm from entering it. The emission monochromator was used to select the optimum wavelength to measure the fluorescent intensity. The intensity of the emission was measured with a photomultiplier tube and accompanying electronics. This light is then directed to the detector that produces a voltage signal proportional to the intensity of the fluorescence.

The fluorescence probe shown in Fig. 2 was a bifurcated optical bundle with 168 fibers spanning from the spectrofluorometer to the test surface. Two optical bundles consisting of 84 fibers each originated from the spectrofluorometer. One of the bundles transmitted the excitation light to the test surface. The other bundle carried the emission from the test surface to the spectrofluorometer. The optical bundles originating from the spectrofluorometer merged into a single probe before entering the test section chamber. The sensor end of the fluorescence probe was sheathed with a quartz tube to protect it from reacting with the R123 test fluid. The 168 fibers of the probe were split evenly between the fibers to transmit the incident intensity (I_0) to the test surface and those to receive the fluorescence intensity (F) from the lubricant on the test surface. The transmitting and sending fibers were arranged randomly with respect to one another.

To reduce the errors associated with the liquid saturation temperature measurement, the saturation temperature of the liquid was measured with two 450 mm long 1.6 mm diameter stainless steel sheathed thermocouples. The small diameter provided for a relatively rapid response time. Nearly the entire length of the thermocouple was in contact with either the test refrigerant vapor or liquid to minimize conduction errors. The tips of the two thermocouples were placed approximately 2 mm above and 150 mm (and 300 mm) to one side of the top of the test surface. This placement ensured that approximately 80 mm of the probe length was in relatively well-mixed liquid near the two-phase fluid above the test surface. To provide for a saturated liquid pool state, the mass of liquid in the pool was large compared to mass of liquid condensed. At the highest heat flux, it would require nearly one hour to evaporate and condense the entire test chamber charge. The lack of a temperature difference between the probe and the

well-insulated, low emissivity, 38 mm aluminum test chamber walls essentially eliminated temperature errors due to radiation.

TEST SURFACE

Figure 4 shows the oxygen-free high-conductivity (OFHC) copper flat test plate used in this study. The test plate was machined out of a single piece of OFHC copper by electric discharge machining (EDM). A tub grinder was used to finish the heat transfer surface of the test plate with a crosshatch pattern. Average roughness measurements were used to estimate the range of average cavity radii for the surface to be between 12 μm and 35 μm . The relative standard uncertainty of the cavity measurements were approximately $\pm 12\%$. Further information on the surface characterization can be found in Kedzierski (2001).

MEASUREMENTS AND UNCERTAINTIES

The standard uncertainty (u_i) is the positive square root of the estimated variance u_i^2 . The individual standard uncertainties are combined to obtain the expanded uncertainty (U). The expanded uncertainty is calculated from the law of propagation of uncertainty with a coverage factor. All measurement uncertainties are reported for a 95 % confidence interval except where specified otherwise.

Heat Transfer

The copper-constantan thermocouples and the data acquisition system were calibrated against a glass-rod standard platinum resistance thermometer (SPRT) and a reference voltage to a residual standard deviation of 0.005 K. The NIST Thermometry Group calibrated the SPRT to two fixed points having expanded uncertainties of 0.06 mK and 0.38 mK. A quartz thermometer, which was calibrated with a distilled ice bath, agreed with the SPRT temperature to within approximately 0.003 K. Both the measured thermocouple electromotive force (EMF) and the measured 1 mV reference were regressed to the SPRT temperature. During a pool-boiling test, the 1 mV reference was measured prior to measuring each thermocouple EMF. The reference voltage was used to account for the drift in the acquisition measurement capabilities over time. Before each test run, the measurements of a thermocouple in the bath with the SPRT were compared. The thermocouple calibration was then adjusted so that bath thermocouple and the SPRT agreed. The mean absolute difference between the thermocouple and the SPRT before correcting for the drift was consistently around 0.07 K over the year of testing. Considering the fluctuations in the saturation temperature during the test and the standard uncertainties in the calibration, the expanded uncertainty of the average saturation temperature was no greater than 0.04 K. Consequently, it is believed that the expanded uncertainty of the temperature measurements was less than 0.1 K. The saturation temperature was also obtained from a pressure transducer measurement with an expanded uncertainty of less than 0.03 kPa. The uncertainty of the saturation temperature from a regression (with a residual standard deviation of 0.6 mK) of equilibrium data (Morrison and Ward, 1991) for R123 was 0.17 K. The saturation temperature obtained from the thermocouple and the pressure measurement nearly always agreed within ± 0.17 K for the pure R123 data.

Figure 4 shows the coordinate system for the 20 wells where individual thermocouples were force fitted into the side of the test plate. The wells were 16 mm deep to reduce conduction errors. Using a method given by Eckert and Goldstein (1976), errors due to heat conduction along the thermocouple leads were estimated to be well below 0.01 mK. The z-coordinate measures the distance normal to the heat transfer surface. The y-coordinate measures the distance perpendicular to the z-coordinate. The origin of the coordinate system was centered on the heat transfer surface with respect to the y-direction. Centering the origin in the y-direction improved the accuracy of the wall heat flux and temperature calculations by reducing the number of fitted constants involved in these calculations. The thermocouples were arranged in four sets of five aligned in the z-direction. Following a procedure given by Kedzierski and Worthington (1993), the size and arrangement of the thermocouple wells were designed to minimize the errors in the wall temperature and temperature gradient measurement.

The heat flux and the wall temperature were obtained by regressing the measured temperature distribution of the block to the governing two-dimensional conduction equation (Laplace equation). In other words, rather than using the boundary conditions to solve for the interior temperatures, the interior temperatures were used to solve for the boundary conditions following a backward stepwise procedure given in Kedzierski (1995).

A backward stepwise regression was used to determine the best model or the significant terms of the solution to the Laplace equation in rectangular coordinates for each data point. Most infinite series solutions should converge within nine terms. The backward stepwise method began by regressing the first nine terms of the Laplace infinite series solution to the twenty measured plate temperatures:

$$T = C_0 + C_1 z + C_2 y + C_3(z^2 - y^2) + 2C_4 zy + C_5 z(z^2 - 3y^2) + C_6 y(3z^2 - y^2) + C_7(z^4 - 6z^2 y^2 + y^4) + 4C_8(z^3 y - zy^3) \quad 1$$

The above “full” model was reduced to its significant terms by removing terms with t-values less than two while maintaining the original residual standard deviation of the full model. Terms were removed one at a time. Regression of the 20 temperatures was done after each term with the smallest t-values was removed. Table 1 provides an overview of the various two-dimensional conduction models that were used to reduce the measured temperatures to heat fluxes and wall temperatures. The top three most frequently occurring models are given with the corresponding percentage of appearance.

Fourier's law and the fitted constants (C_0, C_1, \dots, C_n) were used to calculate the average heat flux (q'') normal to and evaluated at the heat transfer surface as:

$$q'' = \left(\frac{1}{L_y} \int_{-\frac{L_y}{2}}^{\frac{L_y}{2}} k \frac{\partial T}{\partial z} dy \right)_{z=0} = \bar{k} C_1 \quad 2$$

where \bar{k} is the average thermal conductivity along the surface of the plate, and L_y is the length of the heat transfer surface as shown in Fig. 4.

The average wall temperature (T_w) was calculated by integrating the local wall temperature (T):

$$T_w = \left(\frac{1}{L_y} \int_{\frac{L_y}{2}}^{\frac{L_y}{2}} T dy \right)_{z=0} = C_0 \quad 3$$

Siu et al. (1976) estimated the uncertainty in the thermal conductivity of OFHC copper to be about 2 % to 3 % by comparing round-robin experiments. Considering this, the relative expanded uncertainty in the heat flux ($U_{q''}$) was greatest at the lowest heat fluxes, approaching 8 % of the measurement at 10 kW/m². In general, the $U_{q''}$ was relatively constant between 4 % and 5 % for heat fluxes above 25 kW/m². The average random error in the wall superheat (U_{T_w}) was between 0.02 K and 0.08 K. Plots of $U_{q''}$ and U_{T_w} versus heat flux can be found in Appendix A.

Fluorescence

Kedzierski (2001) describes the method for calibrating the emission intensity measured with the spectrofluorometer and the bifurcated optical bundle as shown in Fig. 2 against the bulk lubricant mass fraction. Three glass vessels were each fitted with a glass tube of the same type that was used in the test chamber. Two jars were used to set the lower (0) and upper (100) limits of the intensity signal on the spectrofluorometer. A jar that contained only pure R123 was used to zero the intensity. Because light intensities are additive, the zeroing ensured that the reflected excitation wave and other effects were not attributed to fluorescence. A second jar that contained a 0.5 mass fraction² liquid mixture of R123 and York-CTM was used to set the intensity on the spectrofluorometer to 100. The third jar was used to measure and record the intensity of prepared refrigerant/lubricant mixtures of various concentrations. The third jar was initially charged with approximately 20 g of lubricant and then evacuated for approximately 10 s. Evacuation of the jar and the sample prevented fluorescence quenching by oxygen (Guilbault, 1967). The jar was then charged with approximately 20 g of pure R123 to give approximately a 0.5 mass fraction. Calibration measurements proceeded by successively diluting the mixture with approximately 2 g increments of pure R123.

A single calibration run consisted of measurements for concentrations beginning with a 0.5 mass fraction and diluting to a lubricant mass fraction of 0.05 or less. Prior to each emission intensity measurement for the variable jar, the zero and 100 limits for the emission intensity of the spectrofluorometer were set with the pure R123 jar and the 50/50 jar, respectively. All emission measurements were made at a wavelength of 455 nm with an excitation wavelength of 380 nm. Although, the calibration data was

² Liquid composition assuming that some refrigerant but no lubricant is in the vapor phase.

taken at room temperature, both the pure refrigerant jar and the 50/50 jar were maintained within approximately 1 K of the temperature of the saturated refrigerant in the boiling rig during heat transfer/fluorescence measurements to account for the temperature effect on fluorescence (Miller, 1981).

Figure 5 shows eight different calibration runs using the calibration procedure described above. The solid line depicts the regression of the intensity of the fluorescence emission (F) to the Beer-Lambert-Bouguer law (Amadeo et al., 1971) as a function of the bulk lubricant mass fraction (x_b) and the bulk liquid mixture density (ρ_b):

$$F_c = 116 \left[1 - 10^{-0.00159 x_b \rho_b} \right] \quad 4$$

The average 95% confidence interval for the lubricant mass fraction is approximately ± 0.01 . The width of the confidence interval is a function of the lubricant fluorescence. A greater absolute fluorescence intensity would reduce the scatter in the data.

Because the molar mass of the lubricant is unknown, the surface excess density (Γ) is defined in this work on a mass basis as:

$$\Gamma = \rho_e x_e l_e - \rho_b x_b l_e \quad 5$$

where the l_e is the thickness of the lubricant excess layer. Precedence for reporting the surface excess density in mass units is given by citing the work of McBain and Humphreys (1932) in which they experimentally verified the Gibbs adsorption equation. A non-zero value of Γ implies that an excess layer exists on the surface.

The equation for calculating the surface excess density from the measured fluorescence emission intensity (F_m) for the York-C™ lubricant is (Kedzierski, 2001):

$$\Gamma = \rho_e x_e l_e - \rho_b x_b l_e = \frac{\rho_b x_b \left(1 - \frac{\rho_b x_b}{\rho_L} \right) \left(\frac{F_m}{F_c} - 1 \right)}{\frac{I_{oe}}{I_{ob}} \left(1 + 1.165 \frac{\epsilon}{M_L} x_b \rho_b l_b \right) \frac{1}{l_b} - 1.165 \frac{\epsilon}{M_L} x_b \rho_b \left(\frac{F_m}{F_c} - 1 \right)} \quad 6$$

where the value of $\frac{\epsilon}{M_L}$ was obtained from the fluorescence calibration as 1.089 m²/kg.

The fluorescent intensity from the calibration (F_c) is obtained from eq 4 evaluated at the charged bulk lubricant concentration of test fluid in the boiling apparatus. The l_b is the distance between the probe and the heat transfer surface and $l_b \gg l_e$. The density of the pure lubricant is ρ_L . The ratio of the absorption of the incident excitation in the bulk to that in the excess layer (I_{oe}/I_{ob}) was obtained from the measured absorption spectrum of a 95/5 mass fraction mixture of R123 and York-C™ shown in Fig. 6. Absorption ratios for the 99.5/0.5, the 99/1, and the 98.2/1.8 mixtures were 0.9, 0.82, 0.71, respectively.

Equation 6 was derived while assuming that the excess layer exists at a minimum thickness, i.e., the excess layer is entirely lubricant. Small excess layer mass fractions give excess layers that are unrealistically too thick. For example, the excess layer thickness ranges from 0.7 mm to 1.3 mm for an assumed excess layer mass fraction of 0.03. Two physical mechanisms support a thin, pure lubricant layer: (1) the preferential evaporation of the refrigerant tends to enrich the excess layer in the lubricant phase; while (2) the bubble pumping action of lubricant from the surface tends to minimize the thickness of the lubricant excess layer.

EXPERIMENTAL RESULTS

Heat Transfer

The heat flux was varied from approximately 80 kW/m^2 to 10 kW/m^2 to simulate typical operating conditions of R123 chillers. All pool-boiling tests were taken at 277.6 K saturated conditions. The data were recorded consecutively starting at the largest heat flux and descending in intervals of approximately 4 kW/m^2 . The descending heat flux procedure minimized the possibility of any hysteresis effects on the data, which would have made the data sensitive to the initial operating conditions. Table 2 presents the measured heat flux and wall superheat for all the data of this study. Table 3 gives the number of test days and data points for each fluid.

The R123/mixture was prepared by charging the purger (see Fig. 1) with pure R123 to a known mass. Next, a measured weight of York-CTM was injected with a syringe through a port in the test chamber. The lubricant was mixed with R123 by flushing pure R123 through the same port where the lubricant was injected and releasing the R123 from the purger. All compositions were determined from the masses of the charged components and are given on a mass percent basis. The maximum uncertainty of the composition measurement is approximately 0.02 %, e.g. the range of a 1.8 % composition is between 1.78 % and 1.82 %.

Figure 7 is a plot of the measured heat flux (q'') versus the measured wall superheat ($T_w - T_s$) for pure R123 at a saturation temperature of 277.6 K. The closed circles represent the present R123 "break-in" boiling data while the closed squares represent the present R123 "surface aged" boiling data. Measurements for each data set were made over a period of approximately one month in the same apparatus and for the same surface. The "surface-aged" boiling data was taken after a month hiatus in R123 "break-in" testing. The data differ substantially in the vigorous boiling region (5K superheat offset), but agree closely in the natural convection/boiling region. Apparently, the surface condition has changed such that many nucleation sites have been eliminated for the aged surface. Marto and Lepere (1982) have also observed a surface aging effect on pool boiling data that was sensitive to initial surface conditioning and fluid properties. The present surface was cleaned prior to installation in the test apparatus sequentially with acetone, TarnexTM, hot tap water, and acetone. Following the cleaning process, the surface was exposed to a heat lamp for several hours. It is believed that the superheat offset is not caused by a malfunctioning of the test equipment because no equivalent offset between the measured

saturation temperature and the saturation temperature obtained from the measured pressure was observed. Also, the agreement of low heat flux data for the two periods shows that the measurements are consistent.

The solid lines shown in Fig. 7 are cubic best-fit regressions or estimated means of the data. Two cubic fits were required to cover the low and the high heat flux data. Table 4 gives the constants for the cubic regression of the superheat versus the heat flux for each data set. The residual standard deviation of the regressions - representing the proximity of the data to the mean - are given in Table 5. Note that the residual standard deviation of the high heat flux data differs between the pure R123 and the R123 "break-in" data by about 50 %, i.e., 0.31 K and 0.20 K, respectively. The greater repeatability of the final set of pure R123 data suggests that the surface is operating in the "broken-in" condition. The dashed lines to either side of the mean represent the lower and upper 95 % simultaneous (multiple-use) confidence intervals for the mean. From the confidence intervals, the expanded uncertainty of the estimated mean wall superheat in the low heat flux region and the high heat flux region ranged between 0.17 K and 0.67 K with the mean of the data having a value of 0.24 K. Table 6 provides the average mean wall uncertainty for all of the test data.

Figure 7 shows that the boiling curve for pure R123 at 277.6 K on the plain surface exhibits two characteristic regimes: a natural convection/boiling regime and a vigorous nucleate boiling regime. The regimes are separated by the cessation of vigorous nucleate boiling (CVNB). The CVNB occurs for the pure R123 data at a superheat of approximately 14 K and 20 K for the "break-in" and surface aged data, respectively. The vigorous nucleate boiling regime exists for superheats that are greater than the CVNB condition. Here, the heat transfer is governed primarily by the formation of isolated bubbles within the cavities of the surface. The superheats below the CVNB are insufficient to support vigorous bubble generation. Consequently, natural convection becomes a prevalent mode of heat transfer for superheats below CVNB (low-active-site-density region). In this region, limited bubble activity exists.

Figure 7 also gives the smooth tube boiling curve measured by Webb and Pais (1992) at the same saturation temperature as the present tests. The Webb and Pais (1992) smooth tube superheat and the "surface aged" superheat agree within 3 K for the vigorous-boiling region. The Webb and Pais (1992) smooth tube heat flux data in the natural convection influenced region is approximately 40 % less than the heat flux for the "surface aged" data. Figure 7 also shows the predictions from a free convection correlation for a horizontal plate with the heated surface facing upward which was recommended by Incropera and Dewitt (1985). The predictions are substantially lower than the present measurements and the Webb and Pais (1992) data. This is consistent with the enhancement of the free convection by some nucleate boiling and the upward motion of bubbles.

Figures 8, 9, and 10 plot the measured heat flux (q'') versus the measured wall superheat ($T_w - T_s$) at a saturation temperature of 277.6 K for the 99.5/0.5, 99/1, and the 98.2/1.8 R123/ York-CTM mixtures, respectively. The mean of the pure R123 "aged data" is

plotted as a dashed line. In Fig. 8, comparison of the 99.5/0.5 mixture boiling curve to the mean R123 boiling curve shows that there is little difference between the curves for superheats below 17 K. However, the heat transfer performance of 99.5/0.5 refrigerant/lubricant is greater than that of the pure refrigerant for superheats between 17 K and 21 K. Similarly, the 99/1 mixture boiling curve shown in Fig. 9 illustrates that there is little difference between the pure and mixture curves for superheats below 15 K. However, the heat transfer performance of the 99/1 refrigerant/lubricant is greater than that of the pure refrigerant for superheats between 15 K and 21 K. Figure 10 shows that the mean heat transfer performance of the 98.2/1.8 refrigerant/lubricant mixture is less than that of the pure refrigerant for all superheats. Figures 8, 9, and 10 also show the results of a prediction method, which is discussed in the preceding and developed in Appendix B, that uses the excess layer data as input.

A more detailed comparison of the mixture and the pure fluid heat transfer performance is given in Fig. 11. Figure 11 plots the ratio of the mixture to the pure R123 heat flux (q''_m/q''_p) versus the pure R123 heat flux (q''_p) at the same wall superheat. A heat transfer enhancement exists where the heat flux ratio is greater than one and the 95 % simultaneous confidence intervals (depicted by shaded region) do not include the value one. Figure 11 shows that the R123/ York-CTM (99.5/0.5) mixture exhibits an enhancement for heat fluxes greater than approximately 26 kW/m² and less than approximately 45 kW/m². The CVNB was visually observed to be located near 26 kW/m². Consequently, the addition of York-CTM to R123 improves the heat transfer associated with vigorous boiling more so than it does for low-active-site-density boiling region. The maximum heat flux ratio for the 99.5/0.5 mixture was 1.136 ± 0.015 at 35.6 kW/m². The average heat flux ratio for the R123/ York-CTM (99.5/0.5) mixture for positive heat flux ratios was 1.09.

Figure 11 shows that the R123/ York-CTM (99/1) mixture exhibits an enhancement for heat fluxes greater than approximately 28 kW/m² and less than approximately 43 kW/m². The CVNB was visually observed to be located near 26 kW/m². Consequently, the enhancement characteristics of the 99/1 mixture are consistent with those for the 99.5/0.5 mixture in so much that it is the vigorous boiling region that is enhanced. The maximum heat flux ratio for the 99/1 mixture was 1.074 ± 0.015 at 35.6 kW/m². The average heat flux ratio for the R123/ York-CTM (99/1) mixture for positive heat flux ratios was 1.05.

Figure 11 shows that the R123/ York-CTM (98.2/1.8) mixture exhibits a degradation for all the heat fluxes that were tested with the exception of heat fluxes between 28 kW/m² and 35 kW/m² where the heat transfer may not differ from the pure refrigerant. The CVNB for the mixture was visually observed to be located near 26 kW/m². Recall that the CVNB for pure R123 occurred at approximately 35 kW/m². Consequently, the addition of York-CTM to R123 enhances the boiling site density but this is not sufficient to cause an overall enhancement of the boiling performance due to the reduction in bubble size with lubricant addition. The maximum heat flux ratio for the 98.2/1.8 mixture was 0.98 at 33 kW/m². The average heat flux ratio for the R123/ York-CTM (98.2/1.8) mixture from 20 kW/m² to 54 kW/m² was 0.88.

Fluorescence

Although the heat flux was varied from approximately 80 kW/m^2 to 10 kW/m^2 , fluorescence measurements were limited between 40 kW/m^2 and 10 kW/m^2 to ensure that boiling did not occur below the fluorescence probe. It was believed that bubbles could have misdirected the excitation and the emission lights. Boiling occurred in patches on the surface for the lower heat fluxes. Accordingly, the surface under the fluorescence probe was observed before fluorescence measurements were made to ensure that no boiling occurred under the probe.

Figure 12 is a plot of the measured lubricant excess density versus the heat flux for the three R123/York-C™ mixtures. Solid lines represent the mean of the data. The shaded regions are 95 % confidence intervals for the mean. The green, red, and blue lines, symbols, and shading correspond to the 99.5/0.5, the 99/1, and the 98.2/1.8 compositions, respectively. The expanded uncertainty of the lubricant excess density was estimated from the multi-use confidence intervals to be 0.01 kg/m^2 , 0.02 kg/m^2 , and 0.014 kg/m^2 for the 99.5/0.5, the 99/1, and the 98.2/1.8 compositions, respectively. Table B.1 in Appendix B provides the residual standard deviation for the Γ fit for each mixture.

The lubricant excess density is roughly the mass of lubricant in the excess layer per surface area in excess of the lubricant contribution from the bulk. Consequently, $\Gamma = 0$ implies that no excess layer exists on the surface. Considering this, Fig. 12 substantiates the existence of the lubricant excess layer for most of the data because most of the data, its mean, and the confidence intervals for the mean are all greater than zero. It is questionable as to whether the excess layer exists for the 99.5/0.5 mixture for heat fluxes greater than 33 kW/m^2 .

Figure 12 shows that an increase in bulk lubricant concentration increases the mass of lubricant on the surface to a point. For example, at a heat flux of 23 kW/m^2 , the lubricant excess layer increased from approximately 0.02 kg/m^2 to 0.05 kg/m^2 when the bulk lubricant mass fraction was doubled, i.e., increased from 0.005 to 0.01. However, when the bulk lubricant mass fraction was nearly doubled again (increased from 0.01 to 0.018) no further increase in the lubricant excess density was observed. This may suggest an upper limit for the mass of lubricant that can be maintained in the excess layer. In addition, during the formation of the excess layer, the removal of lubricant for the 0.018 mass fraction mixture must occur at either a much greater rate or with a much different dependence with time than the 0.01 mass fraction mixture for the steady state Γ to remain unchanged.

DISCUSSION

Figure 13 illustrates the influence of the excess layer thickness on the normalized heat flux (q''_m/q''_p) for the range of measured l_e . The values shown in the figure for both the relative heat flux and the thickness are the means of the regressed data for the three mixtures of this study. The maximum heat flux enhancement corresponds closely to the minimum observed excess layer thickness relative to the size of the bubble for each mixture. Consistent with intuition, a build up of lubricant on the surface is detrimental to pool boiling performance.

The importance of the excess layer thickness on pool boiling can be further illustrated with the use of a simple semi-empirical model for refrigerant/lubricant mixtures. The model was developed to show how the lubricant layer can adversely affect heat transfer by flooding the bubble with lubricant. Appendix B provides the details of the model development, which involves both heat transfer and excess density data. Figure 14 shows a schematic of the average departure bubble for each of the three mixtures at the maximum heat flux for each mixture. Note that the model correctly predicts that the departure diameter decreases with increasing lubricant in the bulk liquid (Kedzierski, 1993). The (99.5/0.5) mixture is shown to have nearly the entire bubble diameter in the bulk fluid. Here, the excess layer thickness is two orders of magnitude smaller than the excess layer for the (99/1) mixture. The (99/1) mixture is shown to have approximately half of its departure bubble diameter within the lubricant excess layer. The departure bubble for the (98.2/1.8) mixture forms entirely within the lubricant excess layer. Presumably, heat transfer performance suffers as more lubricant must be displaced from the wall in order to make way for the fresh bulk refrigerant.

CONCLUSIONS

A newly developed fluorescent measurement technique was used to investigate the effect of bulk lubricant concentration on the lubricant excess layer during boiling of R123 and a commercial lubricant (York-C™). A spectrofluorometer was specially adapted for use with a bifurcated optical bundle so that fluorescence measurements could be made perpendicular to the heat transfer surface. The heat transfer surface was a horizontal, roughened, copper flat plate. Larger enhancements are associated with smaller lubricant excess layers relative to the size of the bubble. The lubricant excess surface density was shown to be the smallest for the smallest concentration. The surface density was nearly the same for the two largest concentrations. However, the boiling performance of the largest lubricant concentration mixture was the worst of all the mixtures because its bubbles were the smallest of all the mixtures.

The boiling heat transfer measurements were simultaneously taken with the fluorescence measurements. The heat transfer performance of 99.5/0.5 refrigerant/York-C™ was on average 9 % greater than that of the pure refrigerant. The heat transfer performance of the 99/1 refrigerant/York-C™ was on average 5 % greater than that of the pure refrigerant. The R123/York-C™ (98.2/1.8) mixture heat flux from 20 kW/m² to 54 kW/m² was on average 12 % less than that of pure R123.

ACKNOWLEDGEMENTS

This work was jointly funded by NIST and the U.S. Department of Energy (project no. DE-01-95CE23808.000 modification #A004) under Project Manager Esher Kweller. Thanks go to the following people for their constructive criticism of the first draft of the manuscript: Mr. P. Rothfleisch, Mr. D. Yashar, and Dr. P. Domanski. The author would also like to express appreciation to Mr. G. Glaeser, Mr. V. Basumallick, and Mr. C. Henry of the NIST Building Environment Division for data collection. Furthermore, the author extends appreciation to Dr. W. Guthrie and Mr. A. Heckert of the NIST Statistical Engineering Division for their consultations on the uncertainty analysis. Special thanks

goes to Dr. T. Vorburger of the NIST Precision Engineering Division for making the roughness measurements of the crosshatch surface. Thanks go to the following NIST personnel: Dr. T. Bruno, Mr. D. Plusquellic, and Dr. G. Fraser for consultations on fluorescence and assistance with the measurement of the absorption spectrum for lubricant. Thanks also goes to Dr. D. Ross of the NIST Process Measurements Division for discussions on excess surface density. The York-CTM lubricant that was donated by Mr. K. Starner and York International is much appreciated. Mr. F. Brogna and Mr. R. Collins of Optical Technology Devices, Inc. designed the modification for the spectrofluorometer to accept the bifurcated optical bundle and were essential in discussions concerning its operation.

NOMENCLATURE

English Symbols

A	absorbance
c	concentration, mol/m ³
C	regression constants in eq 1
D	regression constants in Table B.1
F	fluorescence intensity
F_c	fluorescence intensity from calibration (eq 4)
F_m	fluorescence intensity measured from boiling surface
I_o	incident intensity, V
I_t	transmitted intensity, V
k	thermal conductivity, W/m·K
l	path length, m
l_e	thickness of excess layer, m
L_y	length of test surface, m
M_L	molar mass of lubricant, kg/mol
q''	average wall heat flux, W/m ²
r_b	bubble departure radius, m
Ra_L	Rayleigh number based on A_s/p (Fig. 10)
T	temperature, K
T_w	temperature at roughened surface, K
U	expanded uncertainty
u_i	standard uncertainty
x	mass fraction of lubricant
X	model terms given in Table 1
y	test surface coordinate in Fig. 4, m
z	test surface coordinate in Fig. 4, m

Greek symbols

Γ	surface excess
ΔT_s	wall superheat: $T_w - T_s$, K
ΔT_{le}	temperature drop across excess layer, K
ϵ	extinction coefficient, m ² /mol
ζ	fraction of excess layer removed per bubble
θ	dimensionless temperature profile eq B.2
λ	thermal boundary constant in eq B.2
ρ	mass density of liquid, kg/m ³

English Subscripts

b	bulk
e	excess layer
L	lubricant
m	measured
p	pure R123
q''	heat flux

s saturated state
Tw wall temperature
v vapor

Superscripts
- average

REFERENCES

- Adamson, A. W., 1967, *Physical Chemistry of Surfaces*, Interscience Publ., New York, 2nd Ed., p. 353.
- Amadeo, J. P., Rosén C., and Pasby, T. L., 1971, *Fluorescence Spectroscopy An Introduction for Biology and Medicine*, Marcel Dekker, Inc., New York, p. 153.
- Eckert, E. R. G., and Goldstein, R. J., 1976, *Measurements in Heat Transfer*, Hemisphere, Washington, 2nd ed., pp. 9-11.
- Guilbault, G. G., 1967, *Fluorescence: Theory, Instrumentation, and Practice*, Edward Arnold LTD., London, pp. 91-95.
- Incropera, F. P., and DeWitt, D. P., 1985, *Fundamentals of Heat and Mass Transfer*, 2nd ed., John Wiley & Sons, New York.
- Kedzierski, M. A., 2001, " Use of Fluorescence to Measure the Lubricant Excess Surface Density During Pool Boiling," *NISTIR 6727*, U.S. Department of Commerce, Washington, D.C.
- Kedzierski, M. A., 1995, "Calorimetric and Visual Measurements of R123 Pool Boiling on Four Enhanced Surfaces," *NISTIR 5732*, U.S. Department of Commerce, Washington.
- Kedzierski, M. A., and Worthington, J. L. III, 1993, "Design and Machining of Copper Specimens with Micro Holes for Accurate Heat Transfer Measurements," *Experimental Heat Transfer*, Vol. 6. pp. 329-344.
- Kedzierski, M. A., 1993, "Simultaneous Visual and Calorimetric Measurements of R11, R123, and R123/Alkylbenzene Nucleate Flow Boiling," *Heat Transfer with Alternative Refrigerants, HTD-Vol. 243*, H.J. Sauer, Jr., and T.H. Kuehn, Eds., ASME, New York, pp. 27-33.
- Laesecke, A., 2001, Private communications, NIST, Boulder, CO.
- Marto, P. J. and Lepere, V. J., 1982, "Pool Boiling Heat Transfer From Enhanced Surfaces to Dielectric Fluids," *ASME Journal of Heat Transfer*, Vol. 104, pp. 292-299.
- McBain, J. W., and Humphreys, C. W., 1932, "The Microtome Method of the Determination of the Absolute Amount of Adsorption," *J. Chem. Phys.*, Vol. 36, pp. 300-311.
- Miller, J. N., 1981, *Volume Two Standards in Fluorescence Spectrometry*, Chapman and Hall, London, pp. 44-67.

Morrison, G. and Ward, D. K., 1991, "Thermodynamic Properties of Two Alternative Refrigerants: 1,1-Dichloro-2,2,2-Trifluoroethane (R123) and 1,1,1,2-Tetrafluoroethane (R134a)," Fluid Phase Equilibria, Vol. 62, pp. 65-86.

Siu, M. C. I., Carroll, W. L., and Watson, T. W., 1976, "Thermal Conductivity and Electrical Resistivity of Six Copper-Base Alloys," NBSIR 76-1003, U.S. Department of Commerce, Washington.

Stephan, K., 1963, "Influence of Oil on Heat Transfer of Boiling Refrigerant 12 and Refrigerant 22," XI Int. Congr. of Refrigeration, Vol. 1, pp. 369-380.

Webb, R.L. and Pais, C., 1992, "Nucleate Pool Boiling Data for Five Refrigerants on Plain, Integral-fin and Enhanced Tube Geometries," Int. J. Heat Mass Transfer, Vol. 35, No. 8, pp. 1893-1904.

Table 1 Conduction model choice

$X_0 = \text{constant (all models)}$ $X_1 = x$ $X_2 = y$ $X_3 = xy$ $X_4 = x^2 - y^2$ $X_5 = y(3x^2 - y^2)$ $X_6 = x(3y^2 - x^2)$ $X_7 = x^4 + y^4 - 6(x^2)y^2$ $X_8 = yx^3 - xy^3$	
Fluid	Most frequent models
R123 (File: 123pln.dat)	X_1, X_2, X_4, X_5 (124 of 185) 67 % X_1, X_2, X_4, X_6 (21 of 185) 11 %
R123 (File: 123pln2.dat)	X_1, X_2, X_4, X_6 (24 of 68) 37 % X_1, X_2, X_4, X_5 (23 of 68) 31 % X_1, X_2, X_4 (11 of 68) 16 %
R123/York-C™ (99.5/0.5)	X_1, X_2, X_4, X_5 (138 of 245) 56 % X_1, X_2, X_4 (33 of 245) 13 % X_1, X_2, X_4, X_5, X_6 (27 of 245) 11 %
R123/York-C™ (99/1)	X_1, X_2, X_4, X_5 (73 of 90) 81 % X_1, X_2, X_4, X_8 (12 of 90) 13 %
R123/ York-C™ (98.2/1.8)	X_1, X_2, X_4, X_5 (49 of 144) 34 % X_1, X_2, X_4, X_8 (20 of 144) 14 % X_1, X_3, X_4, X_6 (15 of 144) 10 % X_1, X_2, X_4, X_6, X_8 (10 of 144) 10 %

Table 2 Pool boiling
data

Pure R123

File: 123pln.dat

ΔT_s (K)	q'' (W/m ²)
15.49	62727.4
15.28	56954.8
15.24	57668.7
15.23	57460.2
14.56	38710.8
14.44	38294.3
15.81	54260.4
15.78	53939.6
14.60	35042.9
16.32	80003.1
16.30	78769.2
16.29	79460.0
16.02	71899.3
15.98	69554.5
16.49	72993.7
16.46	72643.8
16.42	72675.9
15.89	54797.7
15.84	56102.0
15.81	55572.0
15.19	43239.0
15.18	43526.6
15.17	43517.8
14.67	32353.8
16.74	79528.5
16.71	80517.4
16.70	80512.9
16.04	64927.8
16.04	64927.8
16.02	64925.2
15.93	62669.1
15.70	56762.8
15.68	56637.9
15.67	56155.6
15.22	41141.3
15.23	40735.1
15.18	40308.8
15.19	40288.1
14.65	28870.8
14.60	28653.5
14.55	28693.8
13.68	23503.5
13.70	23438.1
13.66	23336.4
11.39	16554.2
11.34	16672.0
16.73	74572.9
16.66	74619.1

16.66	74482.7
16.20	64724.5
16.19	64132.3
16.12	62425.3
15.76	53983.2
15.73	55766.6
15.76	55732.6
15.25	40498.1
15.22	40227.9
15.14	41262.6
15.16	41050.0
13.34	22602.7
13.37	22214.8
16.80	70666.9
16.80	71175.8
16.80	71422.4
16.60	66764.6
16.57	56745.7
16.54	66422.4
16.19	59449.5
16.20	60454.8
16.28	62287.7
15.76	56003.9
15.76	56178.4
16.84	68867.5
16.82	68859.8
16.81	68543.9
16.21	54598.7
16.17	54652.0
15.46	38126.7
15.40	38019.4
14.60	26402.6
14.73	27388.9
14.70	28595.2
13.45	22591.9
13.64	24113.0
10.84	15998.8
10.84	16017.3
10.80	15729.4
16.87	76664.8
16.48	64065.8
16.38	63409.9
16.32	61380.7
15.61	41301.9
15.53	40856.3
15.47	39894.9
15.33	37529.0
15.29	37086.1
15.27	37100.9
14.39	27473.9
14.41	26661.8

14.32	26799.7
16.71	72964.4
16.70	72885.7
16.68	72797.2
16.12	52678.6
16.11	52610.4
16.09	52469.4
15.20	31624.8
15.20	31330.2
15.38	35111.4
12.98	20044.9
12.89	19889.1
12.88	19934.9
16.79	73022.5
16.75	72718.0
16.73	72571.4
16.29	61681.7
16.31	61667.8
16.14	61906.6
15.31	35091.6
15.40	35886.4
17.12	75360.3
17.05	71905.2
17.05	73114.3
16.69	68294.1
16.70	68134.3
16.71	68015.0
16.29	48216.3
16.10	49173.0
16.10	48969.8
15.73	38426.1
15.72	38323.8
15.70	38263.2
15.57	35833.7
15.59	36460.0
15.57	36671.3
15.42	33108.1
15.40	32847.8
15.38	32928.3
17.05	71905.2
17.05	73114.3
16.69	68294.1
16.70	68134.3
16.71	68015.0
16.29	48216.3
16.10	49173.0
16.10	48969.8
15.73	38426.1
15.72	38323.8
15.70	38263.2
15.57	35833.7

15.59	36460.0
15.57	36671.3
16.97	73460.4
16.97	74198.4
17.02	75802.9
15.67	35238.8
15.59	34477.1
15.60	34730.0
15.12	32468.4
15.08	32737.2
15.08	32414.7
12.41	18818.6
12.40	18761.6

Pure R123
File: 123pln2.dat

ΔT_s (K)	q'' (W/m ²)
20.96	51516.8
20.95	51381.9
20.91	51358.2
19.85	36938.9
19.81	36818.1
19.77	36634.6
15.83	27062.6
15.90	27305.7
15.87	27065.8
13.97	25444.9
13.93	25765.2
20.94	49607.1
21.15	58049.7
20.93	49971.5
20.82	44608.1
20.83	44912.0
20.84	45247.8
20.65	39145.3
20.62	38866.3
20.56	38665.1
18.69	32828.1
18.70	32771.1
18.73	32615.6
13.87	23043.1
13.85	22883.7
21.02	54003.9
21.04	55865.2
21.03	55887.4
20.70	40925.4
20.66	39443.3
20.65	39379.1
20.59	38513.3
20.68	39381.5

20.70	39928.3
19.33	34477.3
19.17	34690.7
19.43	35237.4
16.91	29980.1
16.96	30330.8
21.04	51875.8
21.05	51925.5
21.06	51638.5
20.80	41780.6
20.82	41812.3
20.77	41833.2
16.76	28323.4
16.85	28288.0
16.84	28389.8
11.54	18828.5
11.66	19059.0
21.08	52080.7
21.10	52442.5
21.09	52312.6
14.46	26300.0
14.66	26415.0
14.59	26401.7
14.59	26401.7
12.70	21604.8
12.66	21369.8
12.73	21939.9
21.15	58049.7
20.93	49971.5
21.07	51277.6
21.07	51287.1
21.09	51249.8
19.95	34261.8
20.02	34650.3
20.02	34587.9
15.96	27103.5

R123/York-C™
(99.5/0.5)

File: R123YC5.dat

ΔT_s (K)	q'' (W/m ²)
21.256	59781.1
21.336	54858.8
20.816	49889.4
20.789	50065.4
20.736	50130.3
18.940	38233.6
18.904	38076.5
18.845	38236.1
16.001	29188.8
15.993	29363.4
16.232	30022.3
14.187	25199.6

14.062	25313.2
14.053	25312.9
12.890	22871.6
12.972	23138.4
13.155	20606.5
12.485	20590.6
21.207	56479.7
21.033	57449.7
21.005	57365.8
20.023	45945.4
19.960	45801.7
19.946	45383.5
17.032	31684.4
17.071	31683.5
16.919	31468.5
14.733	27271.6
14.673	27379.1
14.629	27615.4
14.840	27750.8
13.005	23315.7
12.949	23134.5
12.978	23062.4
11.813	20116.2
11.830	20058.8
11.773	20001.7
10.696	17285.8
10.774	17561.2
18.510	38506.1
18.571	38753.8
18.369	36999.8
17.430	34034.6
17.747	34392.8
21.166	56476.5
21.428	50506.1
21.403	50811.4
19.831	41090.4
19.779	41344.3
19.760	41183.0
18.065	33237.3
18.073	33397.9
18.099	33423.7
16.266	29248.6
13.621	23654.0
13.698	23682.8
13.710	23677.3
12.001	19746.2
11.978	19857.3
21.619	50969.9
21.435	56842.4
21.497	51415.9
21.055	51522.8
21.065	51676.6

21.013	52134.2
17.465	31506.6
17.214	30898.8
17.214	30891.9
14.707	25204.4
14.748	25322.3
14.717	25434.2
13.420	22313.6
13.378	21973.3
12.146	19703.3
12.123	19397.8
12.016	19463.8
11.378	17764.5
11.351	17926.3
11.331	17900.3
11.367	17846.1
11.020	17508.9
11.040	17457.4
11.035	17496.0
21.500	59583.1
21.480	59570.6
20.155	43741.6
20.106	43257.2
18.238	33537.4
18.162	33394.3
18.182	33281.3
16.622	29473.2
16.544	29440.9
16.531	29277.8
14.350	24691.1
14.290	24573.6
14.278	24087.3
12.774	21158.1
12.808	21146.2
12.658	20993.0
11.624	18500.7
11.478	18327.1
11.613	18335.4
10.855	16900.2
10.922	17000.6
10.914	16981.7
14.731	24148.0
14.608	23940.2
21.301	54131.1
21.258	54227.2
21.241	53809.0
20.713	46989.0
20.499	45971.3
20.558	47181.7
19.029	36956.4
19.016	36612.3
18.966	36464.6

18.411	34435.9
18.149	33932.4
18.231	34658.1
15.585	27114.0
15.782	27493.0
15.769	26653.9
13.865	23812.2
13.966	23892.3
9.178	15107.7
9.189	15109.0
9.284	15242.6
7.773	12137.5
7.752	12138.6
21.475	52370.1
21.547	53194.8
21.534	53556.8
20.164	41392.7
20.075	40915.8
20.056	41006.6
19.622	37455.7
19.579	37577.9
19.583	37671.3
19.186	36151.9
19.429	37546.2
19.379	37112.5
17.053	30294.7
16.928	30362.1
17.147	30762.4
14.720	25211.1
14.767	26022.9
12.542	21171.6
12.431	21583.4
21.508	49702.1
21.604	51492.3
21.698	52865.3
21.376	49059.0
21.319	48754.0
21.000	45172.9
20.983	44998.2
20.899	45635.2
19.063	35157.3
19.107	35606.0
19.123	35231.6
17.853	32457.0
17.766	31754.3
17.750	32074.4
16.360	29322.9
16.357	29330.3
16.361	29152.9
10.256	16310.3
10.194	16229.0
10.158	16101.6

9.427	14666.7
9.424	14564.4
9.452	14596.3
7.771	12225.9
7.499	11687.2
7.477	11821.0
4.307	5661.0
4.241	6221.7
21.425	54883.9
19.106	37914.6
19.107	37530.7
18.116	33693.6
18.041	33626.8
18.042	33500.7
17.392	31981.1
17.564	32537.2
17.339	31970.3
16.532	29622.5
21.352	55085.3
16.309	29191.8
15.845	28412.4
15.797	28233.6
15.790	27849.7
14.876	25960.0
14.720	25650.6
21.673	52223.6
21.602	52445.2
21.531	52381.7
21.128	48635.1
21.086	48456.1
21.047	48466.7
20.090	42607.8
20.251	43465.0
20.372	44182.8
19.555	39520.6
19.527	38968.1
19.466	39295.9
18.085	33887.7
18.021	33795.4
16.345	28741.1
16.131	28610.7
14.568	25122.0
14.492	24859.5
14.506	24509.6
14.003	23581.4
14.011	23635.1
13.967	23708.2
12.528	21411.6
12.553	21107.4
21.674	55186.7
21.614	55235.6
21.605	55321.2

21.095	48468.2
21.106	47822.2
20.937	46520.5
20.508	43688.0
20.419	43085.4
20.413	42101.1
19.019	35786.2
19.161	37255.1
19.378	38176.4
17.881	33126.3
17.754	32786.0
17.689	32551.2
16.749	30942.5
16.660	30081.1
16.461	29865.7
15.334	27199.9
15.321	27139.8
15.227	26576.3
13.606	23443.8
13.577	23546.1
13.771	23916.4
12.707	21488.8
12.695	21147.3
12.641	21634.1
11.275	18198.7
11.273	18127.6
11.366	18361.2

R123/York-C™ (99/1)
File: R123YC1.dat

ΔT_s (K)	q'' (W/m ²)
21.239	50178.8
21.044	47378.1
21.061	47548.7
16.155	27536.1
16.111	27597.8
16.118	27561.6
13.845	22862.0
13.794	22760.4
13.793	22710.9
12.902	20836.7
12.865	20719.4
12.825	20697.0
12.249	19398.0
12.241	19423.3
11.609	17996.0
11.541	17926.3
11.645	18203.0
21.239	50178.8
21.044	47378.1
21.061	47548.7
21.239	50178.8

21.044	47378.1
21.061	47548.7
16.155	27536.1
16.111	27597.8
16.118	27561.6
13.845	22862.0
13.794	22760.4
13.793	22710.9
12.902	20836.7
12.865	20719.4
12.825	20697.0
12.249	19398.0
12.241	19423.3
11.609	17996.0
11.541	17926.3
21.765	48936.1
21.785	49005.8
21.787	53570.2
21.487	48336.8
21.454	48352.0
21.432	48326.7
20.042	37755.3
20.043	37785.6
20.041	37879.3
17.682	30766.8
17.672	30968.0
17.578	30932.2
16.796	28681.5
16.403	27307.3
14.624	24280.0
14.587	24740.3
15.090	25221.2
13.899	22787.8
13.894	22809.1
13.871	22624.6
13.159	21200.6
13.478	21744.2
13.204	21163.3
12.462	19796.0
12.495	19696.6
12.502	19765.3
12.054	18919.5
16.063	26851.7
21.455	54973.9
21.333	55591.0
21.304	55499.2
20.924	48345.0
20.899	47938.3
20.873	47675.2
20.148	41552.3
20.121	41502.7
20.102	41497.7

19.633	36567.0
19.578	36887.8
19.627	36999.6
17.555	30797.5
17.405	30371.8
17.426	30677.9
16.087	27164.3
16.063	26851.7
16.053	27089.5
14.514	23950.9
14.443	23771.0
13.227	21115.5
13.204	21108.9
21.867	54422.0
21.865	54500.0
21.834	54679.7
21.546	48276.6
21.539	48220.8
21.529	48301.1
18.789	34284.8
19.129	34993.2
19.241	35164.5
17.514	30861.6
17.535	30871.8
17.551	30880.7
16.020	26978.6
16.054	27004.5
15.997	27014.9
14.112	22960.9
13.645	22026.4
13.500	21798.0
13.369	20814.8
13.398	20903.7
13.392	20783.7

R123/ York-C™
(98.2/1.8)
File: R123YC2.dat

ΔT_s (K)	q'' (W/m ²)
22.21	53944.3
22.17	53724.3
22.13	53503.6
21.84	45824.1
21.84	45824.1
21.84	44962.6
21.82	44882.4
21.29	40681.3
21.27	40646.1
21.17	40465.1
20.47	36648.0
20.51	36989.7

20.51	36959.1
19.59	33463.6
19.52	33461.1
19.54	33309.4
18.21	29964.9
22.22	46329.8
22.25	46543.4
22.26	46574.8
22.07	44266.8
22.07	44400.9
22.06	44249.4
21.41	39123.7
21.38	39218.5
21.36	38660.1
20.29	34461.4
20.27	35017.7
20.31	35381.5
19.04	31524.5
18.76	30930.4
18.68	31167.5
18.60	31290.2
18.77	30820.1
18.87	31150.7
17.15	27364.6
17.07	27110.5
16.99	27059.2
16.07	25608.0
22.22	46329.8
22.25	46543.4
22.26	46574.8
22.07	44266.8
22.07	44400.9
22.06	44249.4
21.41	39123.7
21.38	39218.5
21.36	38660.1
20.29	34461.4
20.27	35017.7
20.31	35381.5
19.04	31524.5
18.76	30930.4
18.68	31167.5
18.60	31290.2
18.77	30820.1
18.87	31150.7
17.15	27364.6
17.07	27110.5
16.99	27059.2
16.07	25608.0
16.22	26126.8
15.81	25549.5
14.67	23160.5

14.54	23005.5
14.50	22920.4
13.33	20168.2
13.53	20909.9
13.56	20872.0
12.54	19086.0
12.56	18976.1
12.56	19115.5
10.97	15988.8
22.22	45328.3
22.22	45267.3
22.21	45138.2
21.56	39448.3
18.68	31167.5
21.63	39696.5
20.18	34127.3
20.19	34631.7
20.17	34638.3
18.25	29233.2
18.20	29657.6
18.32	33383.2
16.15	28950.0
16.08	28878.1
16.04	28911.9
14.55	26510.5
14.65	26508.9
14.78	27292.9
13.52	24708.1
13.56	24766.4
22.21	53639.9
22.18	53456.3
22.14	53356.4
21.79	47829.0
21.81	47728.2
21.88	47652.8
16.96	27460.3
16.93	27328.8
16.95	27438.7
14.58	23080.1
14.56	23169.2
14.71	24023.9
13.56	21483.1
13.81	21972.4
13.52	21289.9
12.49	19317.3
12.40	19192.5
12.41	19113.9
11.79	17877.8
12.03	18177.4
11.98	18298.7
10.85	15824.4
10.80	15859.0

10.73	15776.0
9.00	12770.6
9.02	12809.0
22.32	44777.5
22.30	53242.3
22.29	53351.8
22.05	46101.8
21.93	45764.2
21.90	45648.6
20.01	34290.3
19.79	33290.0
19.80	33047.9
18.13	29012.7
17.99	29152.6
17.97	29354.7
15.81	25212.3
15.75	25106.3
14.40	22293.3
14.31	22326.5
14.41	22447.5
13.24	20097.2
13.19	20084.9
13.24	20132.3
11.71	17266.6
11.67	17142.6
11.41	16606.5
11.01	16040.4
11.02	16113.3
11.03	16099.8
9.62	13410.0
9.55	13421.7
22.09	45478.6
21.90	48444.7
20.74	37165.2
19.89	34096.3
17.67	28425.1
17.38	27824.4
19.52	33438.9
17.66	27978.7
15.38	23847.4
15.67	25171.6
15.84	24800.1
13.84	21002.4
13.32	20179.8
13.30	20049.5

Table 3 Number of test days and data points

Fluid (% mass)	Number of days	Number of data points
R123 "break in data"	15	171
R123	6	69
R123/York-C™ (99.5/0.5)	11	245
R123/York-C™ (99/1)	4	90
R123/York-C™ (98.2/1.8)	6	144

Table 4 Constants for cubic boiling curve fits for plain copper surface

$$\Delta T_s = A_0 + A_1 q'' + A_2 q''^2 + A_3 q''^3$$

ΔT_s in Kelvin and q'' in W/m^2

Fluid		A_0	A_1	A_2	A_3
R123	$\Delta T_s \geq 13$ K	7.71421	4.17449×10^{-4}	-7.45117×10^{-9}	4.69661×10^{-14}
"break-in data "	$\Delta T_s \leq 13$ K	4.34389	-3.67068×10^{-4}	8.26988×10^{-8}	-2.14203×10^{-12}
R123	$\Delta T_s \geq 18$ K	-32.2044	3.20480×10^{-3}	-6.42276×10^{-8}	4.28317×10^{-13}
	$\Delta T_s \leq 18$ K	25.3837	-2.12686×10^{-3}	9.53098×10^{-8}	-1.11703×10^{-12}
R123a/York-C™ (99.5/0.5)	$\Delta T_s \geq 19$ K	51.7920	-2.54999×10^{-3}	6.33178×10^{-8}	-4.90908×10^{-13}
	$\Delta T_s \leq 20$ K	1.50894	5.02619×10^{-4}	3.77597×10^{-9}	-1.24206×10^{-13}
R123a/York-C™ (99/1)	$11 \text{ K} \leq \Delta T_s \leq 21.5 \text{ K}$	-0.82896	7.87921×10^{-4}	-5.22161×10^{-9}	-3.32047×10^{-14}
R123a/York-C™ (98.2/1.8)	$9 \text{ K} \leq \Delta T_s \leq 22.5 \text{ K}$	2.98244	3.88456×10^{-4}	9.51211×10^{-9}	-1.92371×10^{-13}

Table 5 Residual standard deviation of ΔT_s from the mean

Fluid	U (K)
R123 $\Delta T_s \geq 13$ K	0.31
"break-in data " $\Delta T_s \leq 13$ K	0.19
R123 $\Delta T_s \geq 18$ K	0.20
$\Delta T_s \leq 18$ K	0.47
R123a/York-C™ $\Delta T_s \geq 19$ K	0.25
(99.5/0.5) $\Delta T_s \leq 20$ K	0.33
R123a/York-C™ (99/1)	0.20
$11 \text{ K} \leq \Delta T_s \leq 21.5 \text{ K}$	
R123a/York-C™ (98.2/1.8)	0.48
$9 \text{ K} \leq \Delta T_s \leq 22.5 \text{ K}$	

Table 6 Average magnitude of 95 % multi-use confidence interval for mean T_w-T_s (K)

Fluid	U (K)
R123 $\Delta T_s \geq 13$ K	0.17
"break-in data " $\Delta T_s \leq 13$ K	0.28
R123 $\Delta T_s \geq 18$ K	0.20
$\Delta T_s \leq 18$ K	0.67
R123a/York-C TM $\Delta T_s \geq 19$ K	0.18
(99.5/0.5) $\Delta T_s \leq 20$ K	0.15
R123a/York-C TM (99/1)	0.13
$11 \text{ K} \leq \Delta T_s \leq 21.5 \text{ K}$	
R123a/York-C TM $\Delta T_s \geq 4.4$ K	0.24
(98.2/1.8) $\Delta T_s \leq 4.4$ K	

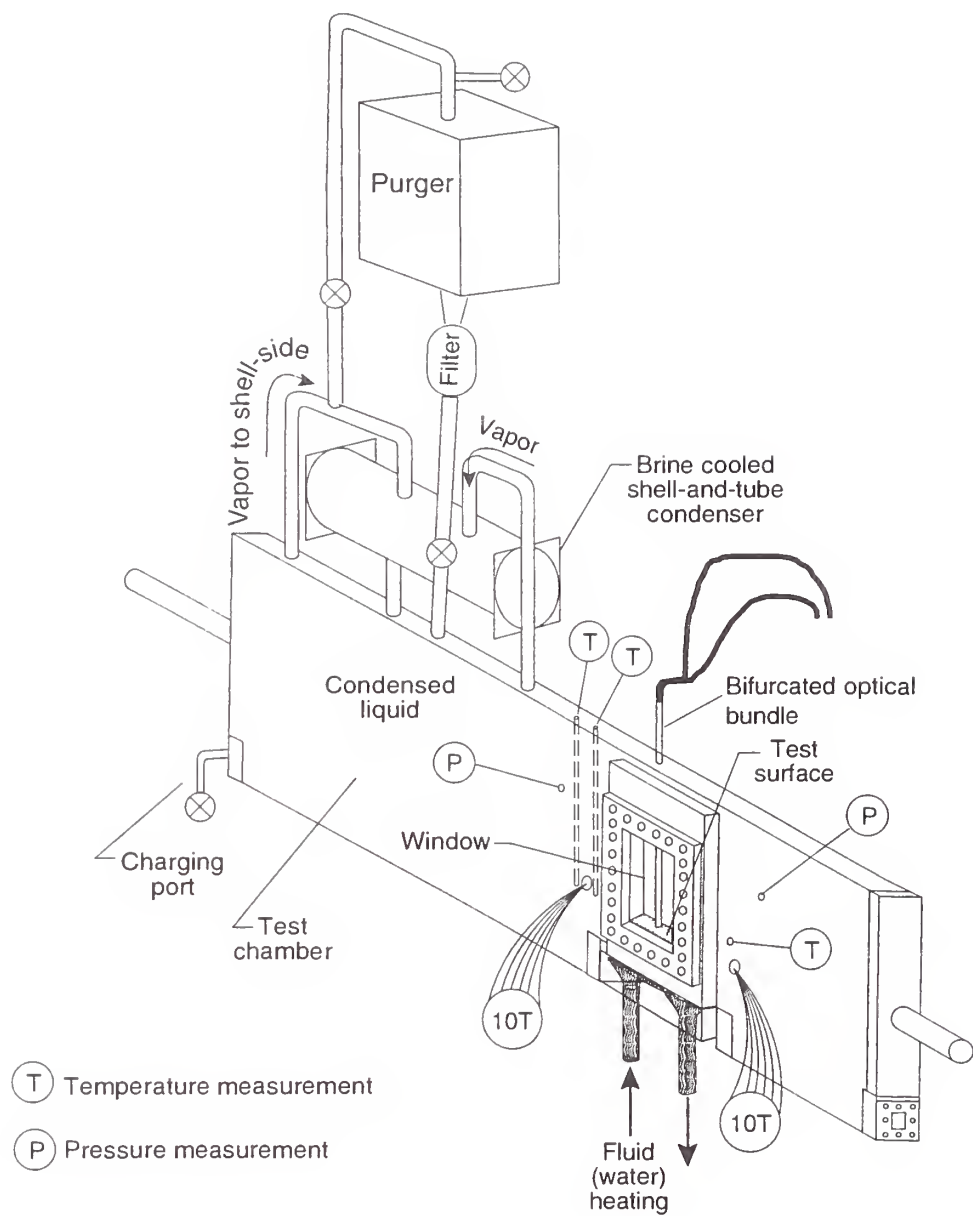


Fig. 1 Schematic of test apparatus

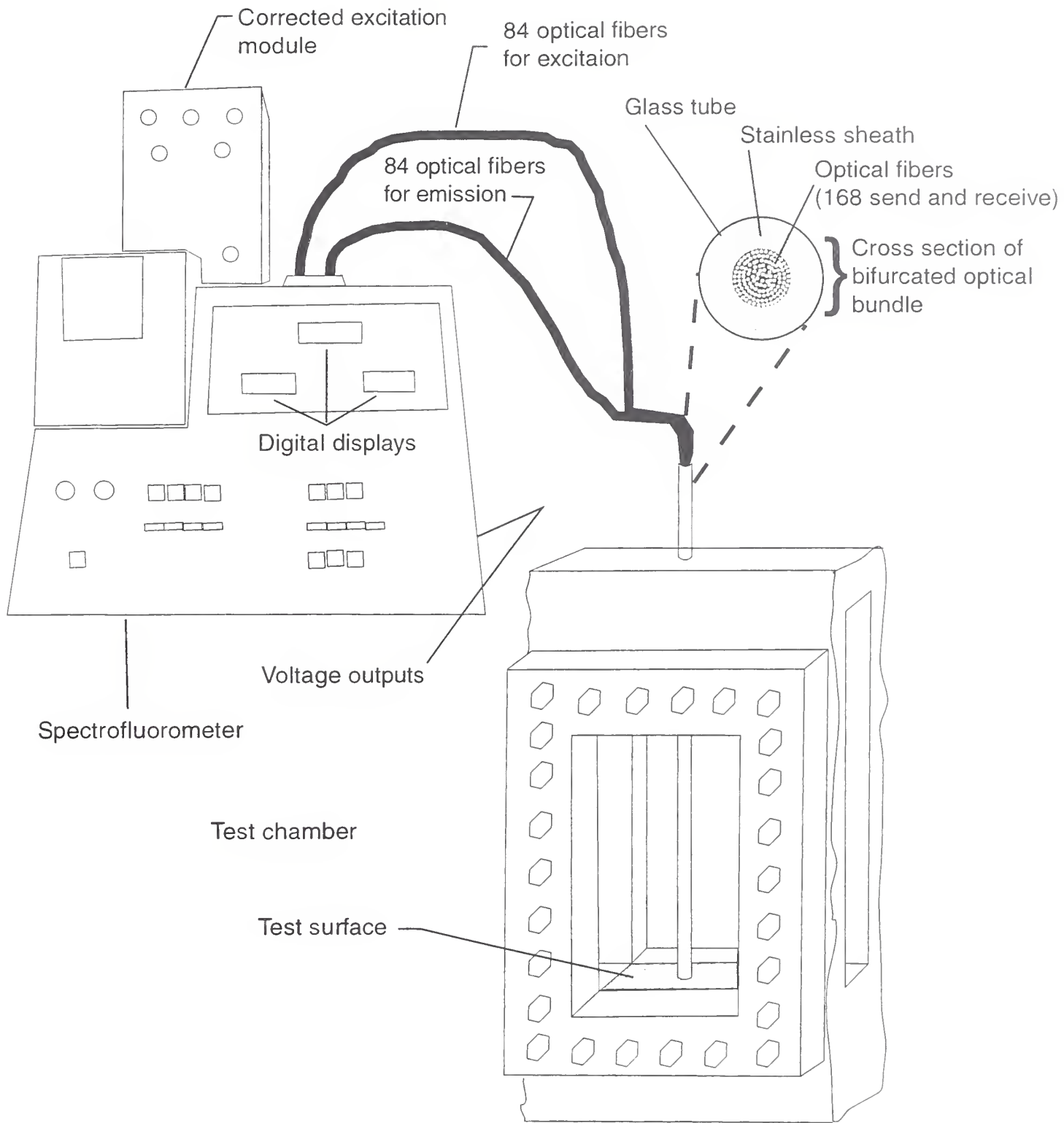


Fig. 2 Schematic of test chamber and spectrofluorometer

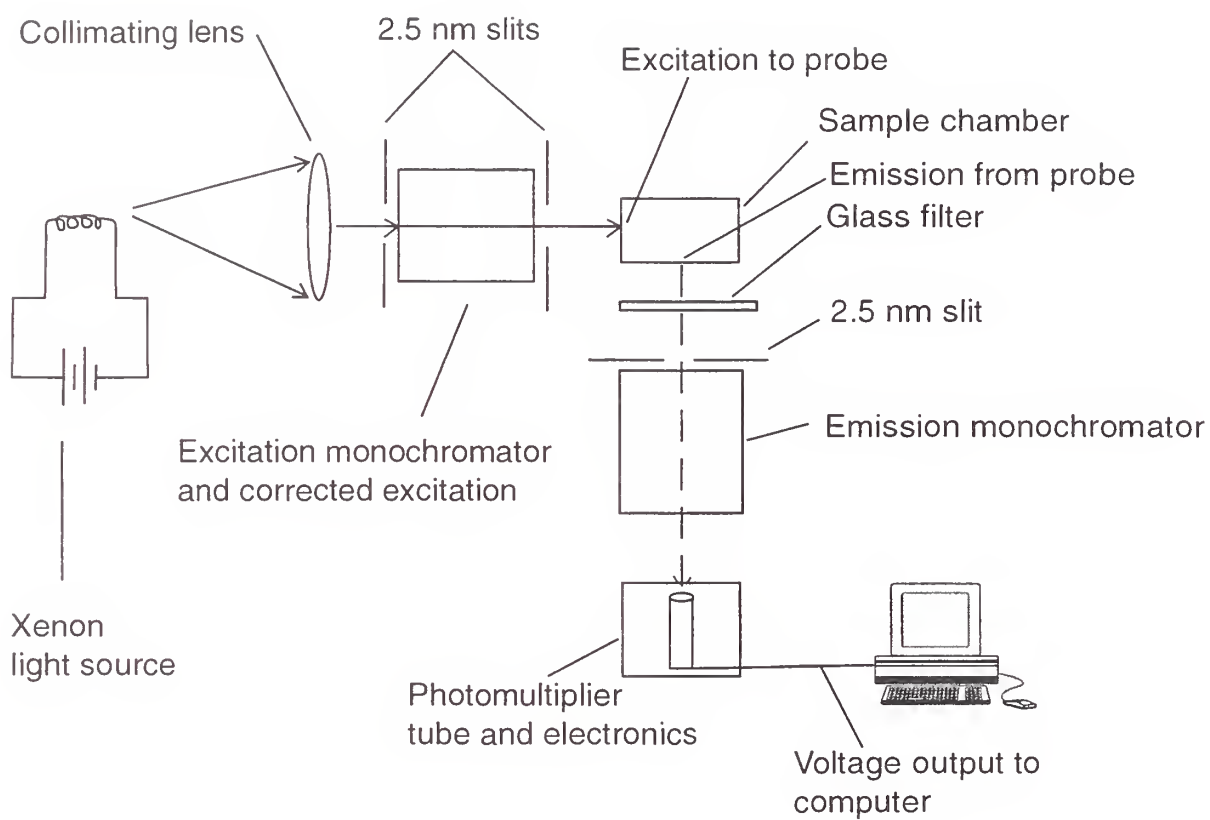


Fig. 3 Schematic of right angle spectrofluorometer

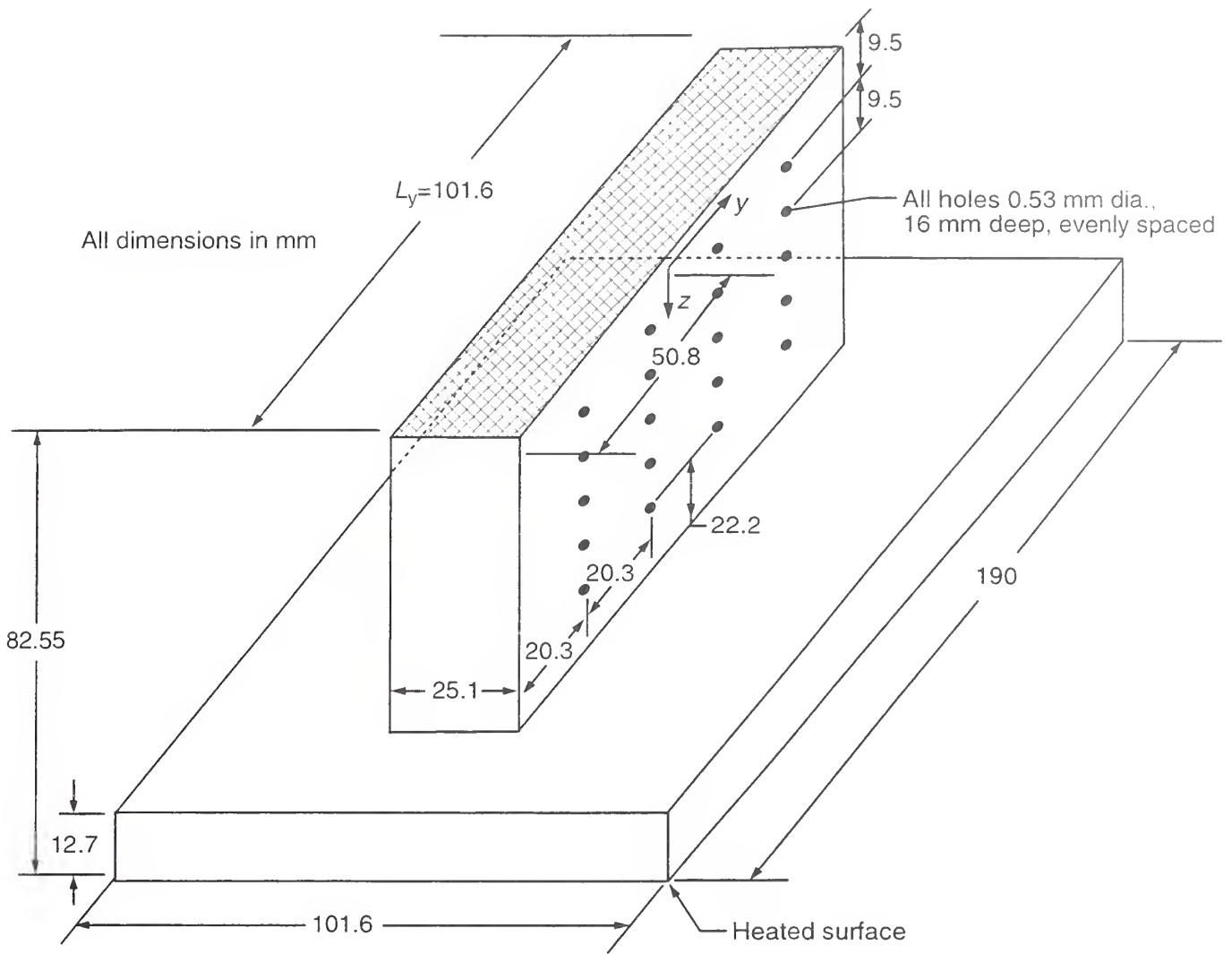


Fig. 4 OFHC copper flat test plate with cross-hatched surface and thermocouple coordinate system

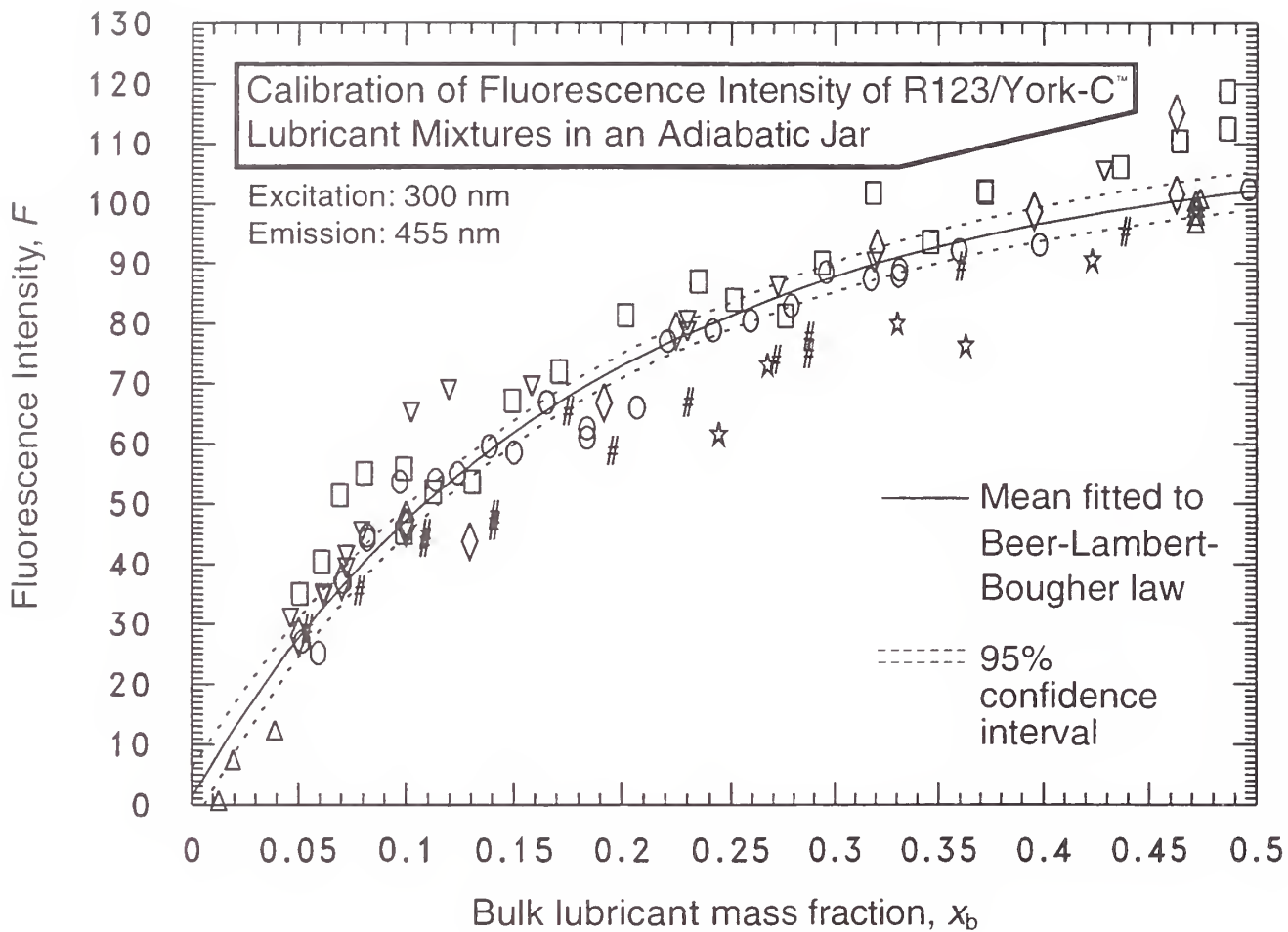


Fig. 5 Fluorescence calibration with $F = 100$ for R123/York-C™ (50/50) jar

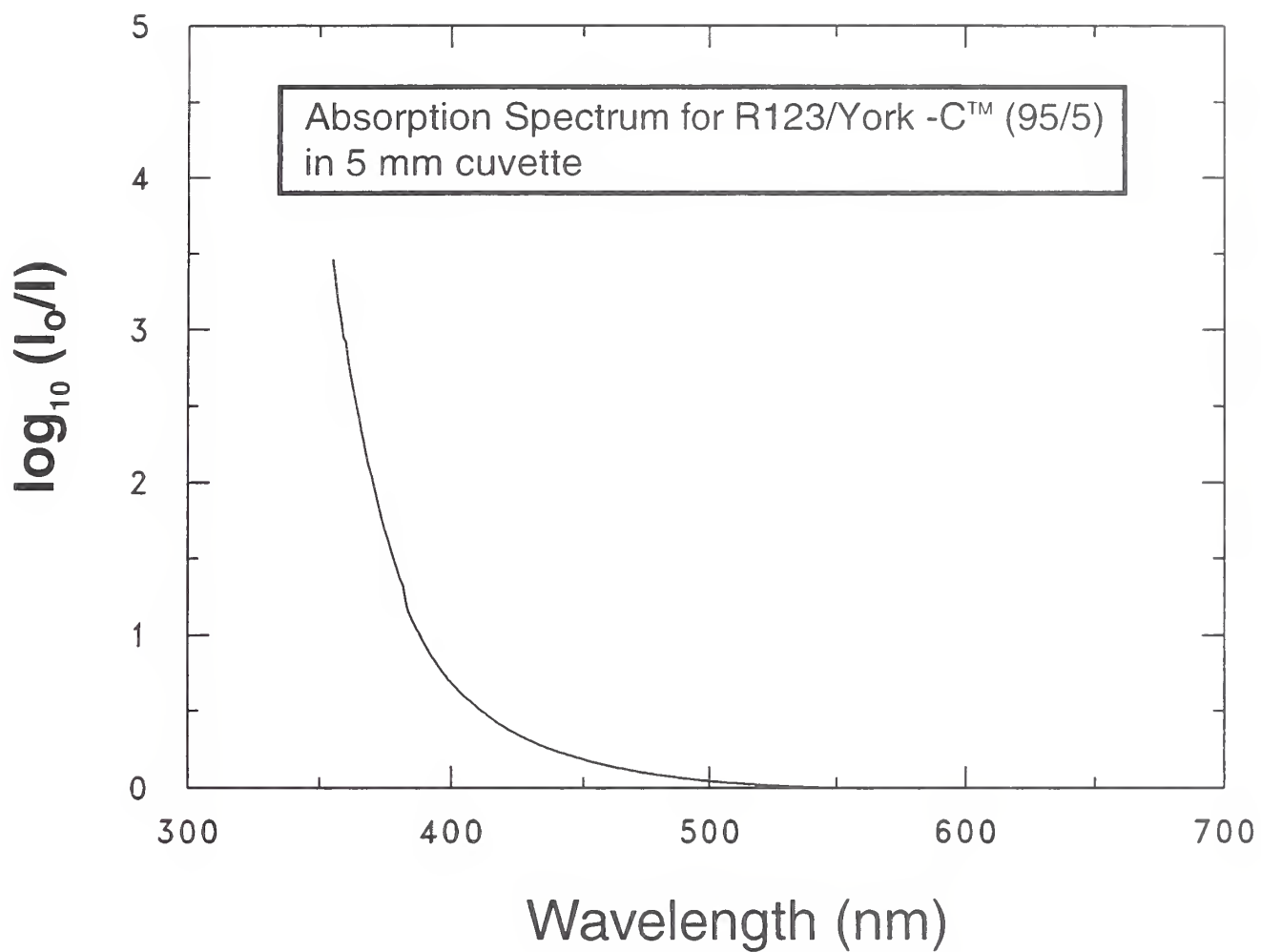


Fig. 6 Absorption Spectrum for R123/York-C™

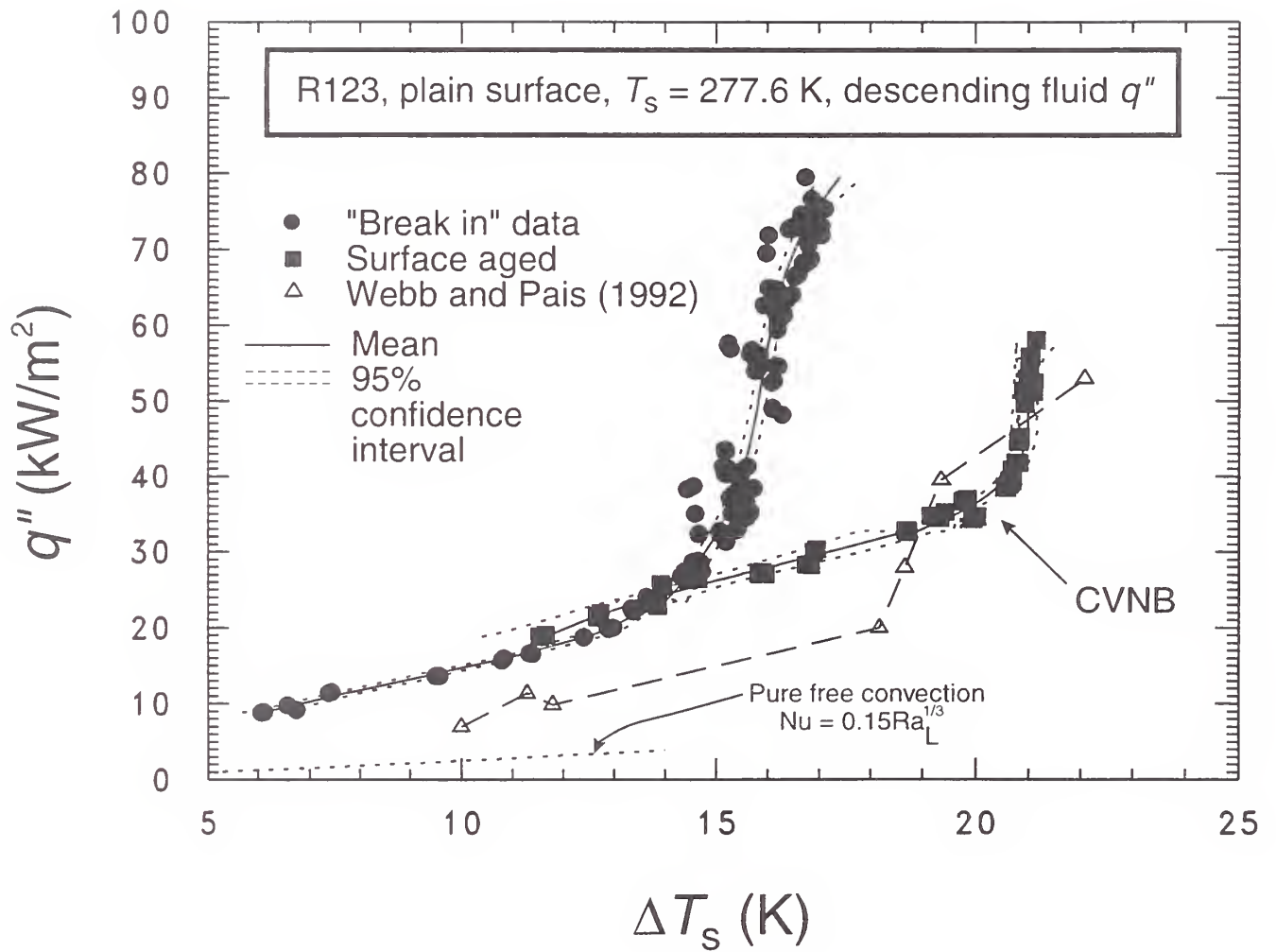


Fig. 7 Pure R123 boiling curves for plain surface

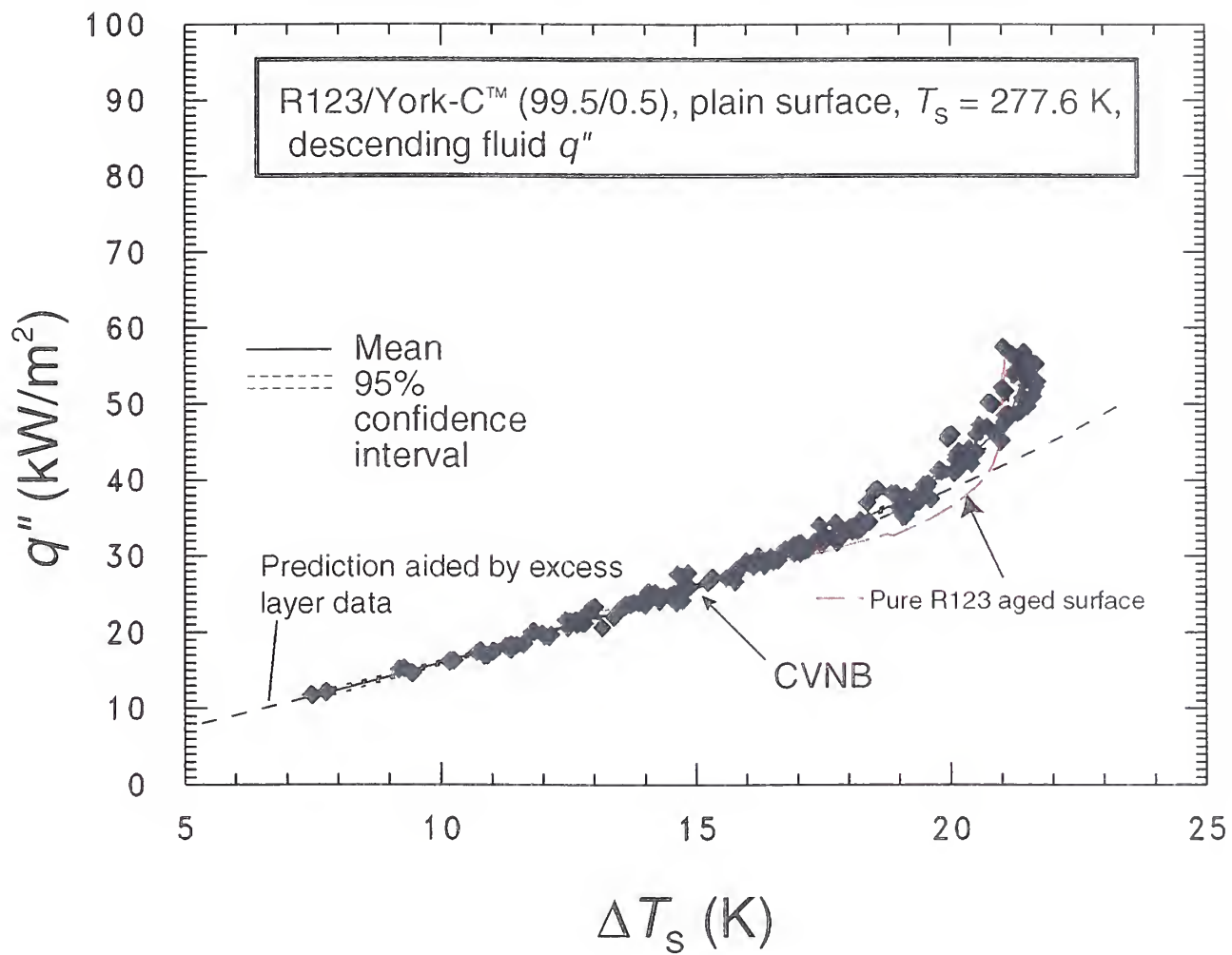


Fig. 8 R123/York-C™ (99.5/0.5) boiling curve for plain surface

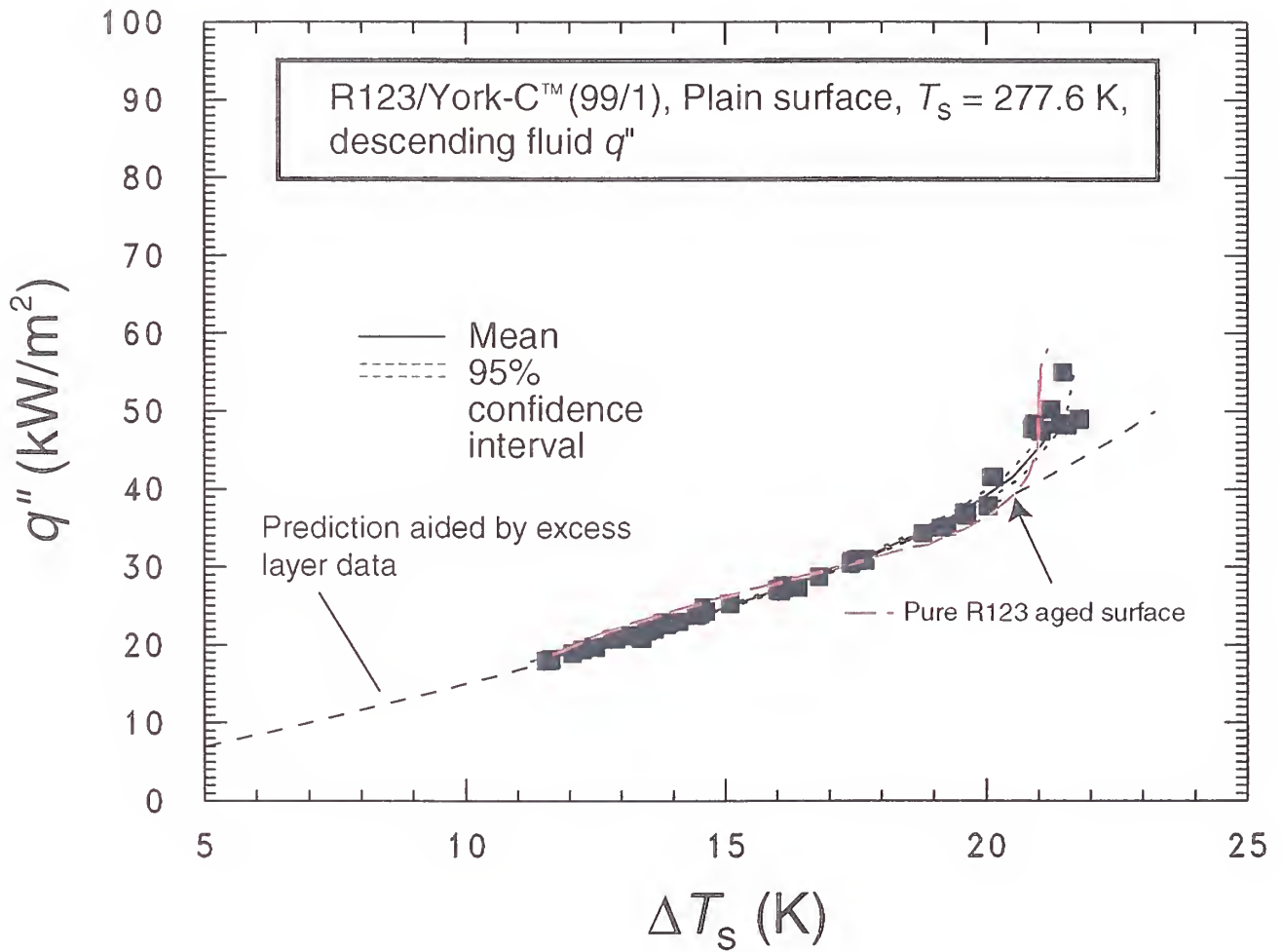


Fig. 9 R123/York-C™ (99/1) boiling curve for plain surface

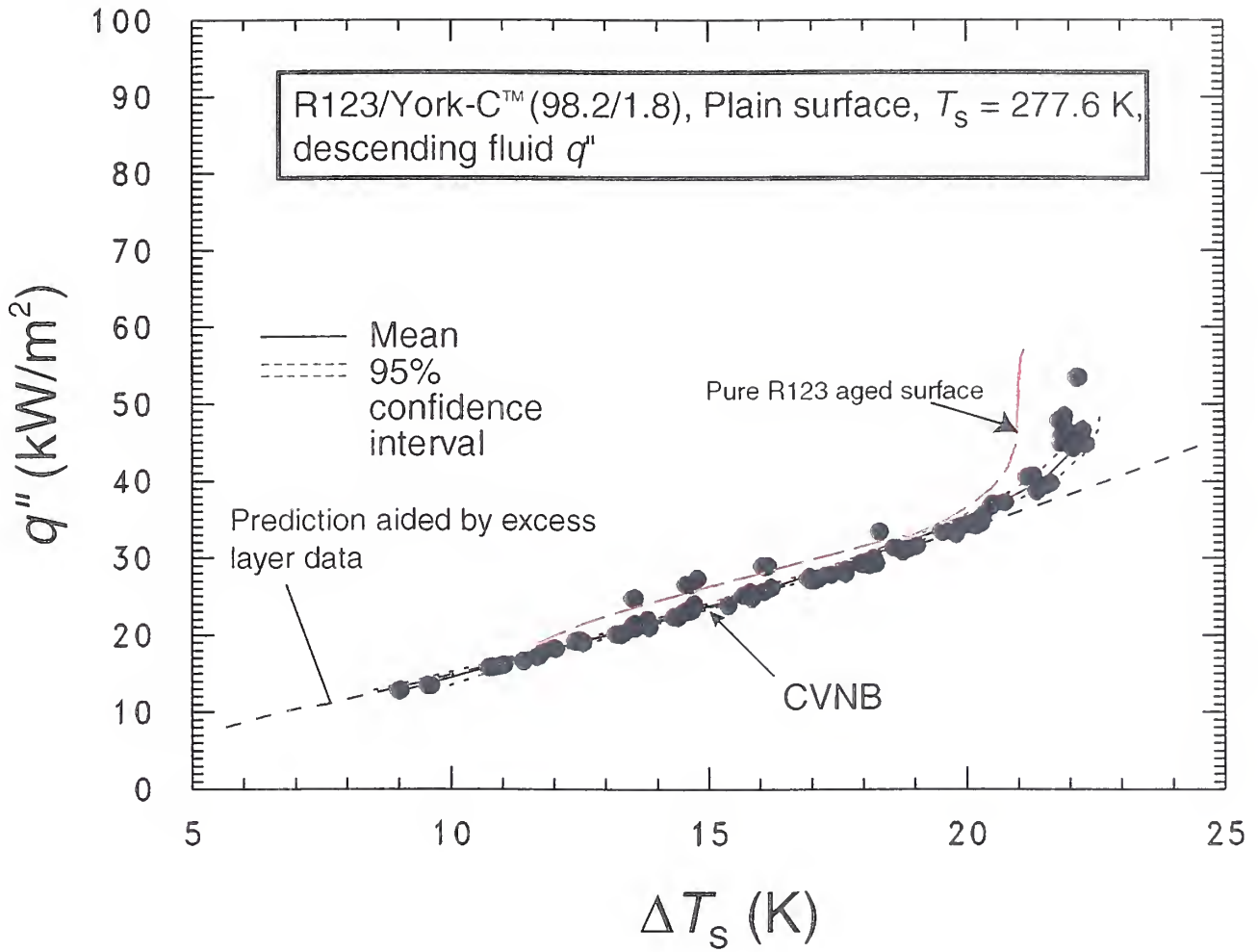


Fig. 10 R123/York-C™ (98.2/1.8) boiling curve for plain surface

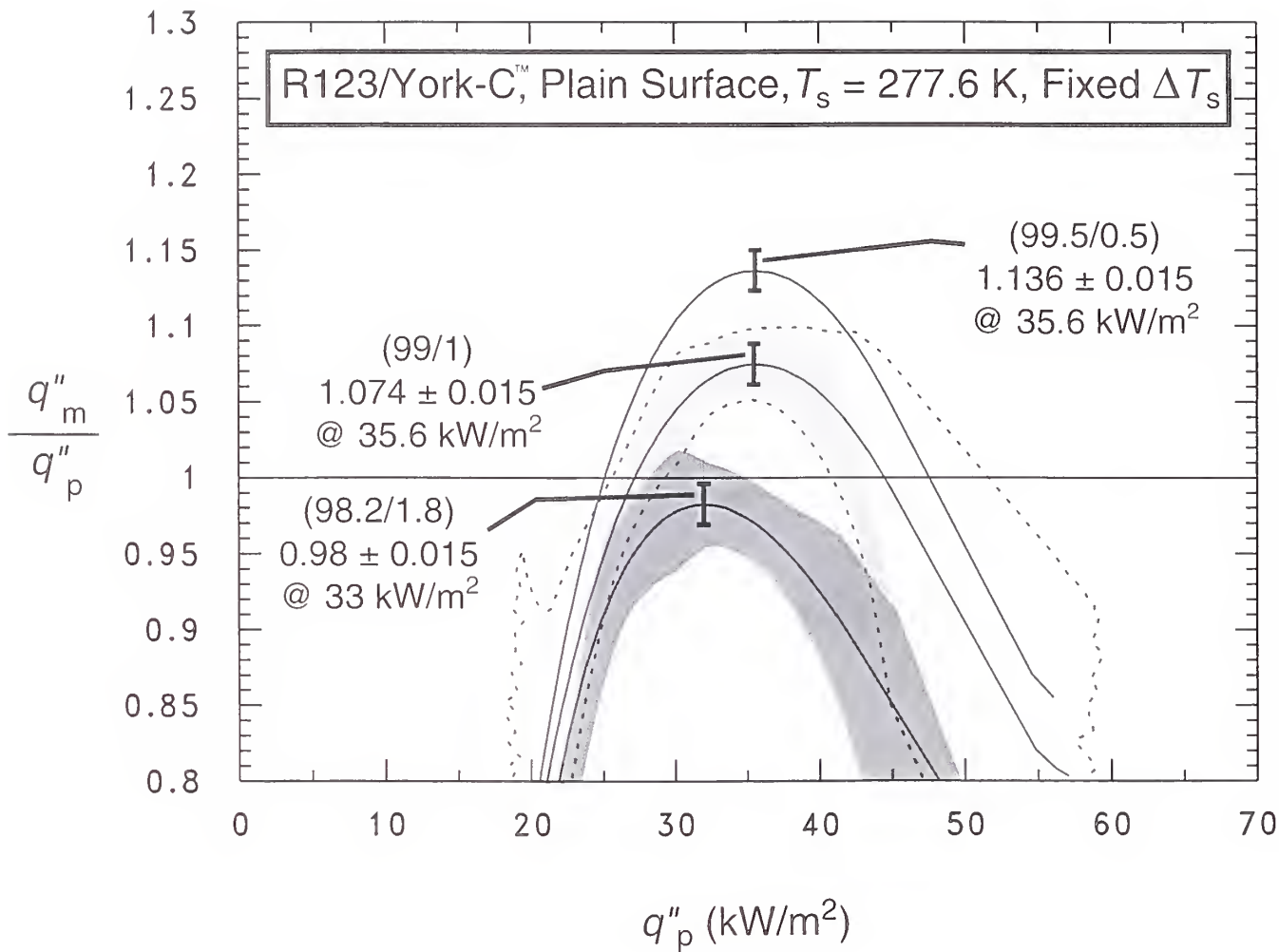


Fig. 11 R123/York-C™ (98.2/1.8) heat flux relative to that of pure R123

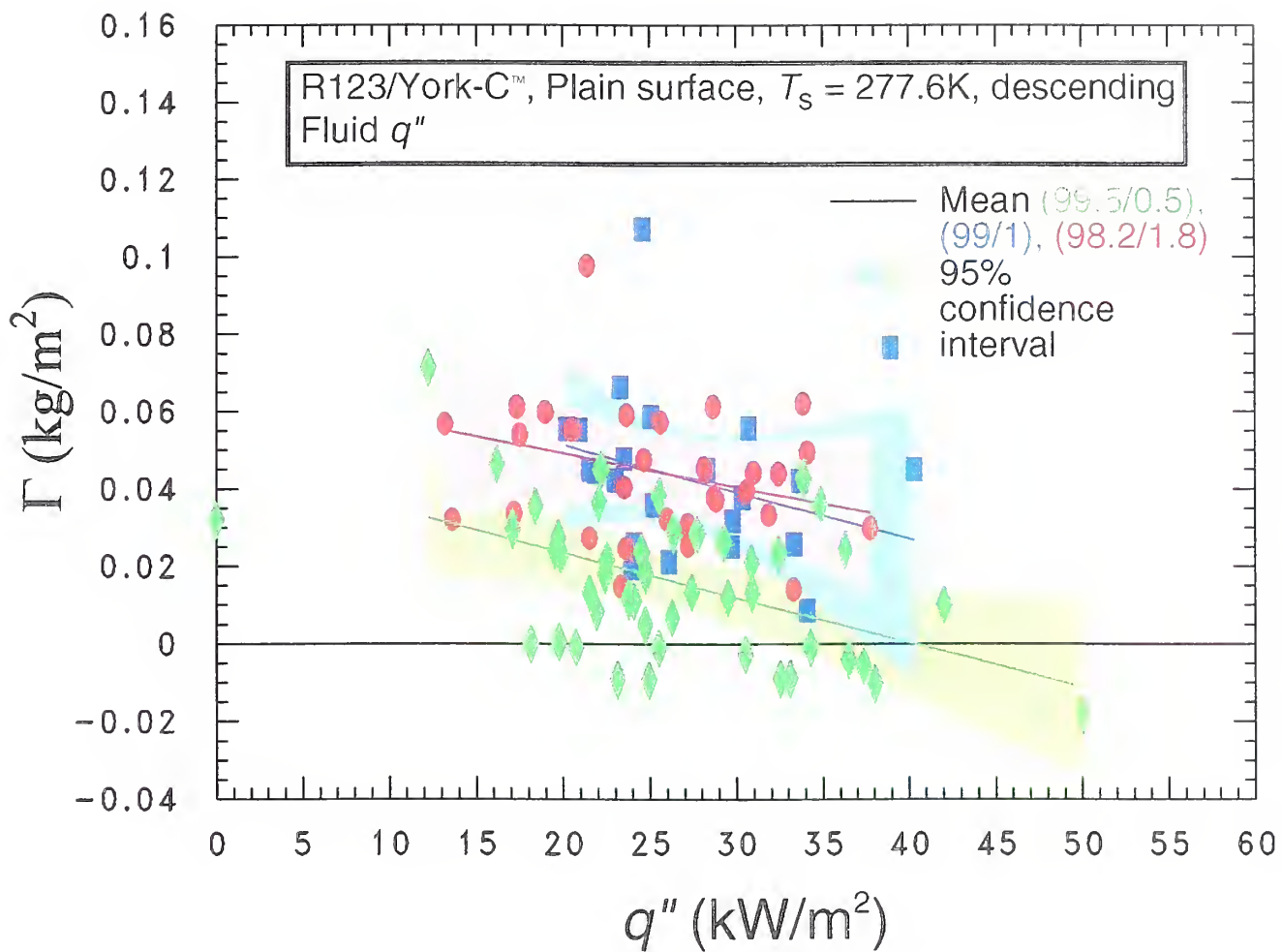


Fig. 12 Lubricant excess surface density for three R123/York-C™ mixtures as a function of heat flux

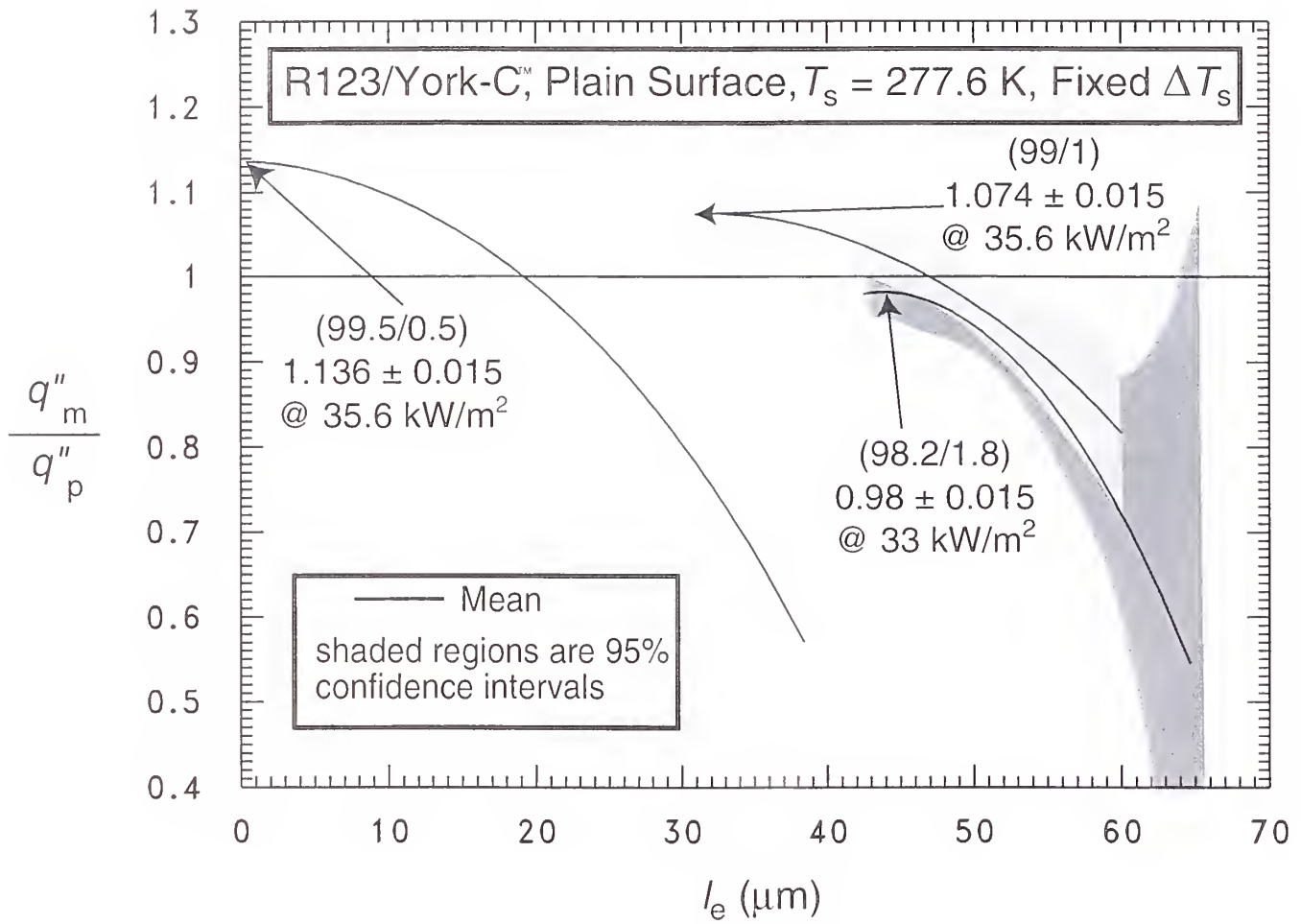


Fig. 13 Influence of excess layer thickness on R123/York-C™ relative heat flux

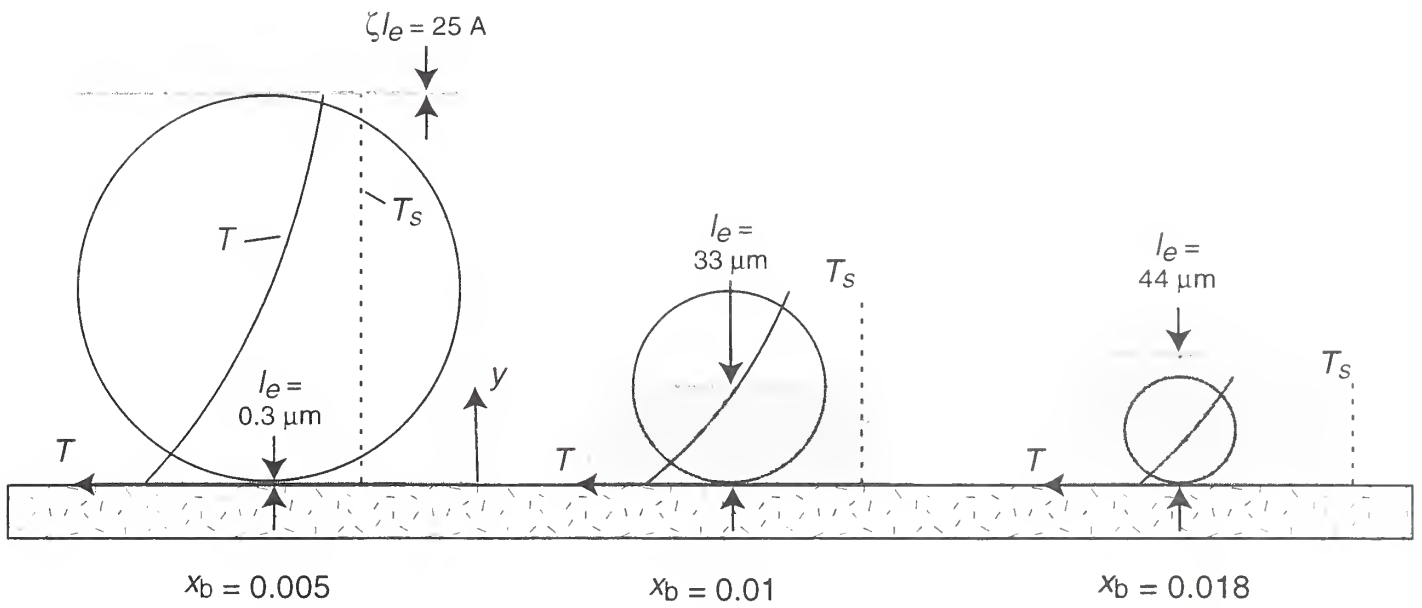


Fig. 14 Schematic of the average departure bubble for three R123/York-C™ mixtures with corresponding excess layers

APPENDIX A

Figure A.1 shows the relative (percent) uncertainty of the heat flux ($U_{q''}$) as a function of the heat flux. Figure A.2 shows the uncertainty of the wall temperature as a function of heat flux. The uncertainties shown in Figs. A.1 and A.2 are "within-run uncertainties." These do not include the uncertainties due to "between-run uncertainties" or differences observed between tests taken on different days. The "within-run uncertainties" include only the random effects and uncertainties evident from one particular test. All other uncertainties reported here are "between-run uncertainties" which include all random effects such as surface past history or seeding. "Within-run uncertainties" are given only in Figs. A.1 and A.2.

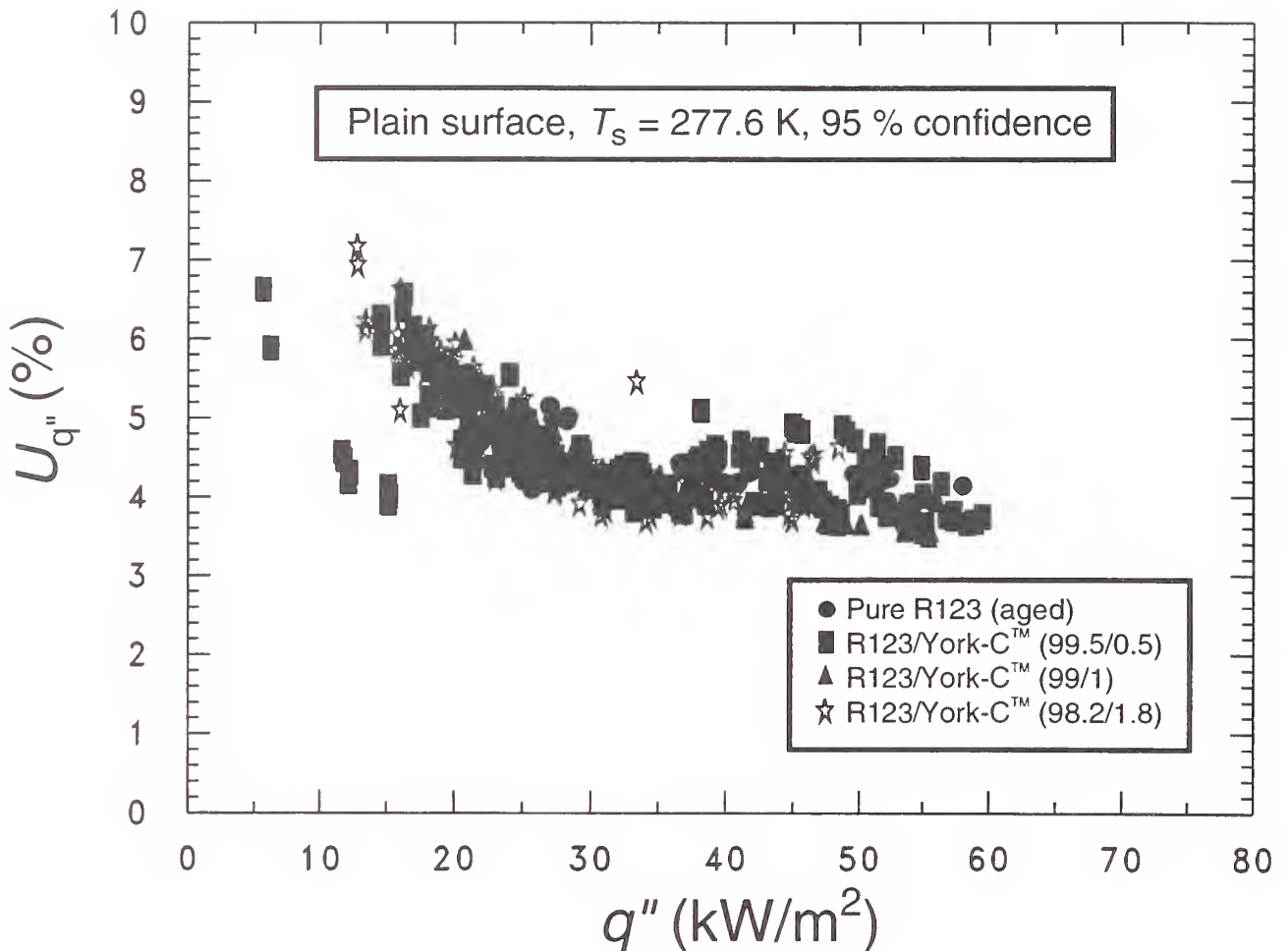


Fig. A.1 Uncertainty in the heat flux at surface for 95% confidence

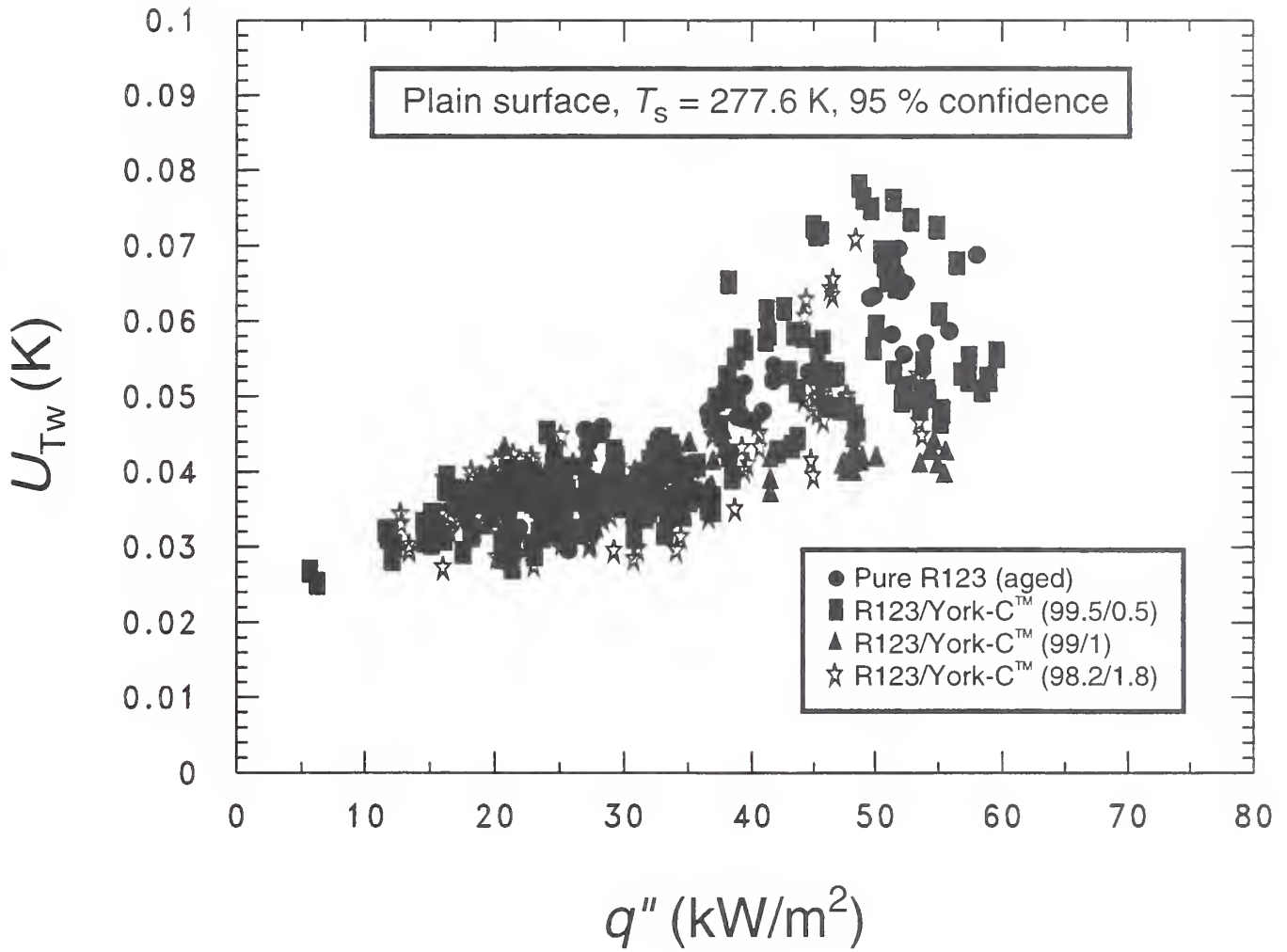


Fig. A.2 Uncertainty in the temperature of the surface for 95 % confidence

APPENDIX B

This appendix outlines the development of a semi-empirical model for the prediction of refrigerant/lubricant pool boiling. The model is fitted to excess surface density and heat transfer measurements. The model relies on three key assumptions: (1) lubricant is lifted from the excess layer as lubricant caps on bubbles, (2) the temperature profile in the thermal boundary layer can be approximated with an exponential function, and (3) the temperature profile within the excess layer is linear.

Figure 14 shows that each bubble removes a fraction (ζ) of the excess layer thickness (l_e) in a volume that is equivalent to that of a lubricant disk with a radius equal to the departure bubble (r_b) and thickness equal to ζl_e . The lubricant that is removed is assumed to reside on the top of the bubble as an adiabatic excess layer of approximately 2 monolayers thick (Adams, 1967), which is approximately 25 Å for lubricant with a liquid viscosity of York-C™ (Laesecke, 2001).

Lubricant is distilled to the excess layer by the boiling of the refrigerant on the wall. The present model assumes that all of the lubricant that is carried to the wall by the bulk liquid/lubricant mixture is deposited on the wall while all of the refrigerant leaves the wall as refrigerant vapor. Writing a mass balance between lubricant deposition and removal and rearranging to solve for the bubble radius yields:

$$r_b = \frac{0.75\zeta l_e \rho_L (1 - x_b)}{x_b \rho_v} = \frac{18.75 \text{Å} \rho_L (1 - x_b)}{x_b \rho_v} \quad (\text{B.1})$$

where ρ_v and ρ_L are the densities of the refrigerant vapor and the liquid lubricant, respectively.

Figure 14 shows the dimensionless temperature profile (θ) of the thermal boundary layer was approximated by the following exponential function:

$$\theta = \frac{T - T_s}{T_w - T_s} = e^{-\lambda y / r_b} \quad (\text{B.2})$$

where T is the temperature of the fluid, y is a coordinate direction measured perpendicularly from the wall, and λ is a constant that is obtained for each mixture from a fit of the measured pool boiling curve.

Equation B.2 is used to calculate the temperature drop in the lubricant excess layer (ΔT_{le}). If the temperature gradient in the excess layer is approximated as linear, Fourier's law can be rearranged to obtain the wall superheat (ΔT_s):

$$\Delta T_s = T_w - T_s = \frac{q'' l_e}{k_L (1 - e^{-\lambda l_e / r_b})} = \frac{q'' \Gamma}{k_L (1 - e^{-\lambda l_e / r_b}) (\rho_L - \rho_b x_b)} \quad (\text{B.3})$$

where k_L is the thermal conductivity of the lubricant, and linear fits of the excess surface density are given in Table B.1. Table B.1 also provides the residual standard deviations and the average multi-use 95% confidence intervals for the fits.

Figures 8, 9, and 10 compare the measured boiling curves for the three mixtures to the model given by eq. B.3. The mean absolute difference between the predicted and measured mean wall superheat is 0.46 K, 0.07 K, and 0.22 K for the (99.5/0.5), (99/1), and (98.2/1.8) mixture, respectively. This comparison was made for the heat flux range for which excess surface density measurements were available. The value of the fitted constant λ was 1.74, 1.09, and 0.57 for the (99.5/0.5) mixture, the (99/1) mixture, and the (98.2/1.8) mixture, respectively.

Table B.1 Constants for linear excess surface density fits for plain copper surface

$$\Gamma = D_0 + D_1 q''$$

Γ in kg/m^2 and q'' in kW/m^2

Fluid	D_0	D_1	Residual Standard dev. (kg/m^2)	Average 95% confidence interval (kg/m^2)
R123a/York-C TM (99.5/0.5) $12 \text{ kW/m}^2 \leq q'' \leq 50 \text{ kW/m}^2$	0.04759	-1.18167×10^{-3}	0.017	0.01
R123a/York-C TM (99/1) $20 \text{ kW/m}^2 \leq q'' \leq 40 \text{ kW/m}^2$	0.08056	-1.33541×10^{-3}	0.02	0.02
R123a/York-C TM (98.2/1.8) $13 \text{ kW/m}^2 \leq q'' \leq 38 \text{ kW/m}^2$	0.06945	-9.46412×10^{-4}	0.018	0.014



